Published in final edited form as:
J Magn Reson Imaging. 2012 October ; 36(4): . doi:10.1002/jmri.23597.

Review of MR Elastography Applications and Recent Developments

Kevin J. Glaser, Ph.D.[1], **Armando Manduca, Ph.D.**[2], and **Richard L. Ehman, M.D.**[1]
[1]Department of Radiology, Mayo Clinic, Rochester, MN, USA
[2]Department of Physiology and Biomedical Engineering, Mayo Clinic, Rochester, MN, USA

Abstract

The technique of MR elastography (MRE) has emerged as a useful modality for quantitatively imaging the mechanical properties of soft tissues in vivo. Recently, MRE has been introduced as a clinical tool for evaluating chronic liver disease, but many other potential applications are being explored. These applications include measuring tissue changes associated with diseases of the liver, breast, brain, heart, and skeletal muscle including both focal lesions (e.g., hepatic, breast, and brain tumors) and diffuse diseases (e.g., fibrosis and multiple sclerosis). The purpose of this review article is to summarize some of the recent developments of MRE and to highlight some emerging applications.

Keywords

Elastography; Elasticity Imaging; Tissue Stiffness; Mechanical Properties; Abdominal Imaging; Neuroimaging

INTRODUCTION

The success of palpation as a clinical tool for the diagnosis of diseases is based heavily on the fact that many disease processes are known to be associated with significant changes in tissue mechanical properties. For example, it is known that many malignant breast cancers are significantly stiffer than benign tumors and healthy fibroglandular tissue. It is also known that the end stage of many liver diseases is cirrhosis of the liver, which results in the liver becoming very hard and nodular. While the ability to detect tissue changes associated with the advanced stage of a disease can be useful for the definitive diagnosis of the disease, more beneficial is the ability to detect tissue changes during the early stages of a disease while the prognosis for treatment is more favorable. The early detection of most cancers, for example, can result in treatments with more favorable outcomes than when the disease is detected at a later stage (1). Unfortunately, due to its qualitative nature and limitation to tissue directly palpable by the physician, palpation by itself has not proven to be a sensitive enough technique to provide this early-stage assessment for many diseases.

The development of elastographic imaging techniques employing ultrasound, optical, and magnetic resonance techniques has come partly from a desire to “palpate by imaging” and thus to improve upon this well-established technique (2–4). Elastographic imaging is used to image the response of tissue to intrinsic and extrinsic stresses, and by analyzing the induced

Corresponding author for the editorial process: Kevin J. Glaser, Mayo Clinic, 200 First Street SW, Rochester, MN, 55905, Phone: 507-538-0757, Fax: 507-284-9778, Glaser.Kevin@mayo.edu. Corresponding author for the final publication: Richard L. Ehman, Mayo Clinic, 200 First Street SW, Rochester, MN, 55905, Phone: 507-284-9770, Fax: 507-284-9778, Ehman.Richard@mayo.edu.

tissue motion, images of qualitative and quantitative measures of tissue mechanical properties (e.g., strain and stiffness) can be produced. While ultrasound-based techniques have provided significant contributions to the field of elasticity imaging for many years (4), the purpose of this manuscript is to review some developments of MR elastography (MRE) and to highlight some recent work which may offer significant clinical utility in the future. However, frequent reference is also made to work incorporating techniques such as ultrasonic imaging, mechanical testing, and biorheology which help to add perspective these MRE results.

REVIEW OF MRE METHODOLOGY

Quantitative elastographic imaging can be considered to consist of 3 steps. The first step is to apply a stress or a source of motion that deforms the tissue. This stress can either come from an internal source, such as heart motion or pulsation of a blood vessel, or from an external, artificial source and the stress may be transient or time harmonic. The second step is to image the tissue response to this stress. This is typically done by measuring tissue displacement or velocity, and numerous ways have been implemented for doing this using ultrasonographic, MRI, and optical techniques. The third step is to use an (inversion) algorithm to process the data to generate images (or elastograms) of tissue mechanical properties.

While a number of static, quasistatic, and dynamic MR elastographic techniques have been developed (5–14), the most common form of MR elastographic imaging is dynamic MRE (11,12) (Figure 1). In this method, time-harmonic motion at one or several acoustic frequencies (typically below about 200 Hz) is introduced into the body through an external vibration system consisting of electromechanical voice coils, piezoelectric bending elements, or pneumatically powered actuators (15,16). The motion of the tissue is recorded using a 1-, 2-, or 3-D phase-contrast MR imaging pulse sequence, which can include gradient-echo (GRE), spin-echo (SE), echo-planar imaging (EPI), and balanced steady-state free precession (bSSFP) techniques (Figure 2). The motion is synchronized with the pulse sequence and the pulse sequence is modified to include additional motion-encoding gradients (similar to flow-encoding gradients in MR angiography). One acquisition produces an image of the component of the true vector tissue motion that is in the direction of the motion-encoding gradients (frequently referred to as a phase, wave, or displacement image). The relative timing (or phase offset) between the motion and motion-encoding gradients is adjusted from one acquisition to another to acquire a series of images of the wave field at different time points, and the direction of the motion-encoding gradients can be changed in subsequent acquisitions to record the full vector motion within the tissue. The temporal and spatial characteristics of the wave field are then studied to provide a meaningful inversion of the wave data to form an image of the tissue mechanical properties.

Numerous inversion algorithms for MRE data have been developed over the years based on different assumptions about tissue anisotropy, viscosity, and boundary effects (17–35). Many of the approaches to inverting dynamic MRE data assume that the tissue can be modeled, at least in local regions, as a linear, isotropic, homogeneous viscoelastic solid undergoing infinitesimal motion absent any body forces. The wave equation for such a material can be written in the temporal-frequency domain as

$$-\rho\omega^2\boldsymbol{U}(\boldsymbol{r},f)=(\Lambda(f)+G(f))\nabla(\nabla\bullet\boldsymbol{U}(\boldsymbol{r},f))+G(f)\nabla^2\boldsymbol{U}(\boldsymbol{r},f), \quad [1]$$

where $\boldsymbol{U}(\boldsymbol{r}, f)$ is the vector displacement field within the object at the position vector $\boldsymbol{r}$ and frequency *f;* $\Lambda(f)$ and $G(f)$ are the frequency-dependent, complex-valued Lamé constants

characterizing the viscoelastic material properties of the object; ρ is the density of the material (typically assumed to be 1000 kg/m^3 for soft tissues); $\omega = 2\pi f$; and ∇, $\nabla\bullet$, and ∇^2 are the gradient, divergence, and Laplacian operators, respectively (4,36,37). This wave equation allows for two types of wave propagation: compression/longitudinal waves and shear/transverse waves. Compression waves in soft tissues in the frequency range typically used for MRE propagate with a very high velocity (around 1540 m/s, primarily affected by Λ) that varies little between different types of tissue. The shear wave velocity (related to the shear modulus G), on the other hand, is typically around 1–10 m/s and can vary significantly between different types of tissue (38,39), thus making the shear properties of tissue more desirable targets for elastographic imaging than the compressional properties.

The presence of compression waves in MRE wave images can confound the desired measurement of the viscoelastic shear properties of tissue. While in theory the wave equation (Eq. [1]) can be solved for both Lamé constants simultaneously, for example by directly inverting the wave equation or incorporating the full wave equation into a finite-element model, the fact that the shear and longitudinal wave speeds (and consequently the two Lamé constants) are orders of magnitude different from each other for tissue makes it impractical to accurately solve for both at the same time (20,22,23,30,31,38,40). Therefore, some effort is usually taken to try to remove the compressional wave motion from MRE data before calculating the shear modulus. The ideal method for the removal of longitudinal wave motion is to calculate the curl of the displacement field first, as (from Eq. [1]) the curl of the displacement field $\boldsymbol{C}(\boldsymbol{r}, f)$ satisfies a simple Helmholtz equation:

$$-\rho\omega^2\boldsymbol{C}(\boldsymbol{r},f)=G(f)\nabla^2\boldsymbol{C}(\boldsymbol{r},f), \quad \boldsymbol{C}(\boldsymbol{r},f)\equiv\nabla\times\boldsymbol{U}(\boldsymbol{r},f). \quad [2]$$

In practice, calculating the curl can amplify noise in the measured data and requires 3D measurements of all 3 components of the motion, which may take a prohibitively long time to acquire for some applications.

In tissue, compression waves have a much longer wavelength than shear waves. Therefore, a more flexible, though sometimes less effective, alternative to calculating the curl to remove the compression waves is to use a highpass filter to suppress the low-frequency compression waves while preserving the high-frequency shear waves. While the spectral nature of the wave data and the characteristics of the filter may prevent a perfect separation of the two types of wave motion, thus biasing the inversion results, this type of filter can be applied to datasets without sufficient information for the curl operation to be performed (such as 2D data or data with only 1 motion-encoding direction). It is also important to note that if only 2D data are acquired, there is an implicit assumption that the shear waves are propagating wholly within the selected imaging slice. Any obliquity between the wave propagation direction and the orientation of the imaging slice leads to a bias in the estimation of the mechanical properties of the tissue because the apparent wave propagation differs from the true wave propagation.

The shear wave velocity c_s is related to the complex shear modulus G by

$$c_S=\sqrt{\frac{2|G|^2}{\rho(\Re(G)+|G|)}}, \quad [3]$$

where $|G|$ and $\Re(G)$ indicate the magnitude and real part of the complex-valued quantity G, respectively (20,37,41). The shear wave speed equation reduces to $\rho c_s^2 = G$ if the material is purely elastic and thus has zero viscosity (i.e., $\Im(G)= 0$, where $\Im(G)$ is the imaginary part

of G). In a typical viscoelastic material which exhibits attenuating and dispersive characteristics, the shear modulus is dependent on the frequency of motion in the object and is thus a function rather than a single value.

In the literature, several different forms of the viscoelastic properties of tissue are reported. Some inversion algorithms calculate only local wavelength or wave speed (e.g., the local-frequency estimation (LFE) and phase-gradient algorithms (17)), which is related to the complex shear modulus via Eq. [3]. The wave speed itself can be reported as the measure of tissue mechanical properties, as is done in several ultrasound elasticity techniques (4). The wave speed can also be reported as an effective shear stiffness, defined as ρc_s^2, which represents the shear modulus of a purely elastic material that exhibits the observed wave speed. In tissue exhibiting only a modest amount of attenuation, this is not too different from the real part or the magnitude of the complex shear modulus. Other algorithms (e.g., direct inversions of the differential equations and finite-element models (17,20,22,23,30,31)) can truly recover the complex shear modulus, which can be used to report both the elastic and viscous properties of the tissue. If MRE is performed at multiple frequencies, then the calculated wave speeds or complex shear moduli at the different frequencies can be fit to a rheological model, such as the Voigt model or a spring-pot model, to obtain additional information about the tissue (26,42–45). While determining the multifrequency viscoelastic properties of tissue offers a more detailed description of the tissue, it is not clear if there is a significant clinical benefit to this information. For example, a significant decrease in brain tissue stiffness in patients with normal pressure hydrocephalus compared to normal volunteers has been observed with both single- and multifrequency MRE measurements (46), and the ability to differentiate grades of hepatic fibrosis is comparable using single- and multifrequency MRE (47).

HEPATIC MRE

The liver can respond to direct or indirect injury with the development of inflammation and fibrosis, which can eventually develop into cirrhosis (48–50). Liver cirrhosis, which has a 50% 5-year mortality, is characterized by a loss of liver function and the liver becoming very firm and nodular. Cirrhosis can also cause additional complications such as ascites and varices. There are numerous causes of liver fibrosis including fatty liver disease, chronic viral infections, alcohol abuse, and autoimmune disorders. Studies have shown that patients with various liver diseases can reverse the impact of the disease on the liver with treatment (51,52), so monitoring the changes of the liver is important not only for fibrosis and inflammation staging, but also for gauging the success of treatment. Currently, liver biopsy is the gold standard for assessing hepatic fibrosis, but it has been shown to have significant risks for patients, as it is an invasive procedure, and it is also subject to sampling errors (53,54). Therefore, a number of noninvasive imaging techniques have been developed to help diagnose and stage hepatic fibrosis (55,56).

Transient ultrasound elastography (TUE, Fibroscan) has emerged as a useful tool for the assessment of liver fibrosis (57,58). The technique uses a combination force and ultrasound probe which is capable of delivering a brief mechanical excitation and imaging the internal tissue displacement due to the pulse. The propagation of the induced wave front can be studied to yield the shear wave speed (or equivalently the shear/Young's modulus or shear stiffness) of the tissue. Applied to liver imaging, TUE has shown a correlation between liver stiffness and the degree of liver fibrosis (57,59,60). While TUE is a simple, fast, and inexpensive procedure, it has also suffered from a number of limitations, namely that the technique is limited to imaging within an acoustic window through an intercostal space, it only samples a small portion of the liver (at a depth of 2.5–4.5 cm within the liver below the

acoustic window), and it has difficulty producing sufficient displacement of the liver in obese patients and in patients with ascites (57,61).

MRE has also been pursued with great interest recently as an alternative or complement to TUE. In several animal models, MRE has shown a correlation between liver stiffness and the degree of hepatic fibrosis (21,62–64). In one of these studies, intraperitoneal injections of carbon tetrachloride were used to induce hepatic injury and fibrosis in rats (62). In another study, a mouse model of autosomal recessive polycystic kidney disease was used to produce progressive hepatic fibrosis (21). In both of these studies, hepatic stiffness correlated with fibrosis extent assessed with picrosirius red staining which indicated that MRE-based hepatic stiffness measurements could be useful for staging and monitoring hepatic fibrosis development.

Several patient studies investigating the capability of MRE for staging liver fibrosis and comparing MRE to TUE have shown that MRE performs as well as or better than TUE while incorporating more liver tissue and not being as limited by obesity and ascites (47,65–74). For example, ROC analysis in one such study of 35 normal volunteers and 50 patients indicated that MRE had a 98% sensitivity and a 99% specificity for differentiating normal livers from all grades of liver fibrosis, and had a 86% sensitivity and a 85% specificity for differentiating patients with mild fibrosis from those with moderate and severe fibrosis (66). One recent application of dynamic hepatic MRE has been as a surrogate for liver biopsy to assess fibrosis in patients with arthritis and other inflammatory diseases undergoing treatment with methotrexate (MTX), which is known to be linked to liver toxicity and is normally monitored with routine biopsies (75–77). As a complement to dynamic MRE, a quasistatic MR tagging technique has also been shown to have potential as a means to measure fibrosis. In a study by Watanabe et al., 22 patients were imaged using a cine-tagging technique which measured the natural deformation of the liver at several time points between full inspiration and full expiration (i.e., no external source of vibration was required) (78). The deformation data were used in an analysis to calculate the “bending energy” of the tissue, a qualitative measure of the strain of the tissue drawn from an analogy of the bending of thin sheets. While not a direct measure of tissue mechanical parameters, the results indicated that the strain was significantly larger (indicating softer tissue) in the patients with F0 fibrosis than in patients with F1 or greater fibrosis. In studies using a similar MR tagging technique to measure cardiac-induced strain in the liver, normal subjects have demonstrated significantly higher hepatic strains than patients with cirrhosis (79,80).

Figure 3 shows MRE examinations performed in 2 subjects. The images in the top row are of a healthy volunteer with no known liver disease. The images in the bottom row are of a patient with steatohepatitis and biopsy-proven fibrosis and inflammation. The patients were imaged in the axial plane while lying supine with 60-Hz vibrations applied to the abdominal wall via a pneumatic actuator placed on the rib cage, as performed by Yin et al. (66). The shear wavelength in the fibrotic liver is much longer than it is in the healthy liver, and the elastograms show that the fibrotic liver is much stiffer than the healthy liver. Figure 3 demonstrates the sensitivity of MRE to diffuse liver disease. Hepatic stiffness is also increased by other pathological properties such as necroinflammatory activity (81–85). Recently, it has been shown that elastography is sensitive to the initial inflammation and cell injury that results in some diseases before the actual development of fibrosis. Results from an MRE study of a rat model of nonalcoholic steatohepatitis (NASH) induced using a choline-deficient diet showed that hepatic stiffness increased before the development of fibrosis and correlated with myofibroblast activation (85). A prospective study involving 12 normal volunteers and 64 patients with chronic liver disease evaluated with MRE reported a significant difference in the mean stiffness of nonfibrotic liver tissue with and without inflammation (3.46 vs. 2.8 kPa, respectively, $p=0.002$) (86). In a study of 22 patients being

evaluated as potential liver donors, a correlation between biopsy-detected inflammation and MRE-assessed liver stiffness was observed (87). The mean liver stiffness of the tissue with inflammation was significantly higher than for the normal tissue (3.28 vs. 2.15 kPa, $p<0.0001$). The preponderance of the current MRE and US elastography literature indicates that hepatic stiffness is affected by fibrosis and necroinflammatory effects, while steatosis alone has little effect (81,85,88–90). The parallel effects of necroinflammation and fibrosis on hepatic stiffness are fortuitous in that they promote early detection of nonalcoholic steatohepatitis with MRE (88). Further research is needed to ascertain whether it may be possible to differentiate the effects of necroinflammatory activity and fibrosis with MRE techniques, such as through the use of rheologic models.

While a significant health problem of its own, cirrhosis of the liver is also linked to the development of hepatocellular carcinoma (HCC), which has a high mortality risk world wide (91,92). Improved techniques for diagnosing and monitoring hepatic tumors could offer significant benefits for managing this disease. While a number of MRI, CT, and ultrasound techniques currently exist for diagnosing HCC, incorporating additional information about the mechanical properties of suspicious lesions may improve the ability to help differentiate malignant from benign hepatic lesions. In a preliminary study investigating the properties of hepatic lesions, malignant liver tumors were shown to be significantly stiffer than benign tumors and fibrotic and normal hepatic tissues (93). This study of 44 lesions included 14 metastasis, 12 HCC's, 5 cholangiocarcinomas, 1 hepatic adenoma, 9 hemangiomas, and 3 focal nodular hyperplasias. It was found that a stiffness threshold of 5 kPa could be used to differentiate the malignant tumors from the benign tumors, suggesting that MRE may have promise for differentiating benign from malignant liver neoplasms. In a similar study using acoustic radiation force impulse (ARFI) elastography to measure the shear wave speed in 60 focal hepatic lesions, a cut-off of 2 m/s (i.e., a shear stiffness of 4 kPa) provided a positive predictive value and specificity of 89% and 81%, respectively, for discriminating these lesions (94). In other studies, viscosity has been shown to be an indicator of hepatic tumor malignancy. In a study of 76 patients with 79 tumors (42 benign, 37 malignant), the loss modulus of the benign tumors (0.99 ± 0.63 kPa) was significantly lower than for the malignant tumors (1.97 ± 1.44 kPa; $p<0.001$) (95). In another study of 100 liver tumors (40 benign and 60 malignant in 63 patients), it was shown that the viscosity information obtained using MRE offered improved diagnostic accuracy over just stiffness information or contrast enhancement information alone (area under the ROC curve (AUC) = 0.81, 0.72, 0.68, respectively) (96).

Chronic liver disease can also affect normal physiology in a number of ways due to the complex interaction between the liver, spleen, pancreas, and gastrointestinal tract via the hepatic portal system. For example, the development of portal hypertension can lead to splenomegaly, gastroesophageal varices, and a significant risk of hemorrhages (97). TUE has been used to investigate the link between hepatic stiffness, portal hypertension, and esophageal varices (98–101). In these studies, increased hepatic stiffness was correlated with increased central venous pressure, significant portal hypertension (assessed with the hepatic venous pressure gradient), and high-grade esophageal varices. While in one preliminary MRE study of 16 healthy volunteers, splenic stiffness was not well correlated with hepatic stiffness or arterial blood pressure (102), another study involving 12 normal subjects and 38 patients observed a significant correlation between hepatic and splenic stiffness that may be indicative of the response of the spleen to an increase in portal pressure (103). Other preliminary research has demonstrated a dynamic component of hepatic stiffness that, while not changing in healthy subjects, is significantly increased postprandially in patients with advanced liver disease which may also be indicative of abnormal regulation of portal blood flow (104–106). The ability to measure hepatic and splenic stiffness using MRE could result

in a noninvasive method for assessing portal hypertension and monitoring changes in portal pressure during disease progression and treatment.

BREAST MRE

Breast cancer is the most frequently diagnosed type of cancer in women, and the second leading cause of cancer deaths in women after lung cancer (107). The 5-year relative survival rate for women with breast cancer is well over 90% when diagnosed at a localized stage, but is significantly lower at more advanced stages (107). This emphasizes the importance for the early diagnosis and staging of breast cancer. While mammography is the only imaging technique recommended for routine breast cancer screening, mammography has limited sensitivity and specificity, especially in certain groups of women with mammographically dense breast tissue (108). Contrast-enhanced MRI (CE-MRI) is recommended for breast cancer surveillance of certain populations of high-risk women, and the sensitivity of the technique has been reported to be nearly 100%. However, the specificity of CE-MRI for breast cancer is still low, which results in a large number of unnecessary biopsies being performed (108–110). Since it is known from mechanical studies that many malignant breast lesions are significantly stiffer than benign lesions and healthy fibroglandular tissue (111,112), MRE and ultrasound elastography have been investigated as supplemental techniques for obtaining additional important information about tissue stiffness in vivo and noninvasively which can be used to improve the overall diagnostic accuracy of breast examinations.

A number of ultrasound elastography studies have been performed to determine the benefit of including elasticity information with conventional x-ray and ultrasound mammography examinations to improve breast cancer diagnosis. In one study of 111 women, real-time freehand elastography was found to have comparable diagnostic performance to ultrasound mammography (113). Similar diagnostic accuracy was found in a study of 193 women with 129 benign lesions and 64 malignant lesions in which ultrasound elastography had a sensitivity, specificity, and AUC of 96.9%, 76%, and 0.884, respectively, while for B-mode ultrasound using BI-RADS classification they were 57.8%, 96.1%, and 0.820, respectively (114). In another study of 232 patients, ultrasound elastography was found to be better than ultrasonography and comparable to mammography for differentiating benign and malignant lesions. The combination of ultrasonography and ultrasound elastography together yielded the best results for detecting cancer with a sensitivity of 90% and a specificity of 96% (115). In a study of 100 women with nonpalpable breast masses, ultrasound elastography and conventional ultrasonography were found to have comparable diagnostic performance (116). Using a technique called supersonic shear imaging (SSI), the stiffness of malignant lesions was found to be significantly higher than for benign lesions in a study of 46 women with 48 lesions (28 benign, 20 malignant) (117).

Preliminary studies with MRE have also shown the potential for using MRE to improve breast cancer diagnosis. In an early study involving 6 healthy women and 6 patients with known breast cancer, MR elastograms depicted breast carcinomas as regions of high shear stiffness that were, on average, about 4 times stiffer than the surrounding fibroglandular tissue (118). In a similar study involving 15 healthy volunteers, 15 patients with malignant tumors, and 5 patients with benign lesions, malignant lesions were found to be significantly stiffer than benign lesions, normal breast parenchyma, and adipose tissue (119). Early work looking at the correlation between MRE and CE-MRI in a study involving 20 patients showed good distinction between benign and malignant lesion stiffness which agreed with the morphologic and dynamic data (120). A more recent study involving 68 patients with 39 malignant lesions and 29 benign lesions, and using a more sophisticated elastographic inversion algorithm, reported that while CE-MRI alone had a sensitivity of nearly 100%, but

a specificity of 40% and an AUC of 0.88, the elastography results alone provided an AUC of about 0.91, and the combination of CE-MRI and MRE resulted in an AUC of around 0.96 (28). A similar prospective study of 57 patients with lesions previously detected by palpation, mammography, ultrasonography, or MRI, (57 total lesions, 37 malignant) found that improved diagnostic accuracy could be achieved using a combination of MRE and CE-MRI compared to using just CE-MRI (AUC = 0.96 vs. 0.93) (121).

In Figure 4, MRE exams were performed on a patient with a fibroadenoma and another with an invasive carcinoma. The MRE data were collected with the patient lying in the prone position with the transducer for the mechanical vibrations applied along the lateral side of the breast slightly compressing it. Vibrations were supplied at 65 Hz and the acquisition was performed using a 2-mm isotropic volume 128 x 128 x 14 mm. Each series shows MR magnitude images from the MRE acquisition and reconstructed stiffness and viscosity images showing the distribution of mechanical properties throughout the breast. The fibroadenoma has similar stiffness and viscosity to the normal fibroglandular and adipose tissues of the breast, while the carcinoma is significantly stiffer and more viscous than the fibroadenoma and other breast tissues.

SKELETAL MUSCLE MRE

Muscle undergoes a number of active and passive changes in mechanical properties during normal function, and changes in these properties can be associated with certain conditions, like stroke and Parkinson’s disease (122,123). In vivo assessments of muscle mechanical properties could have applications for sports training, physical therapy, and monitoring disease progression and response to treatment. Current results involving MRE and ultrasound-based assessments of muscle stiffness have highlighted the diverse behavior of the properties of muscle that must be understood to gauge the impact of various diseases. Numerous ultrasound-based muscle elasticity imaging techniques have been developed to image various muscle groups under different amounts of loading and to explore muscle viscosity, dispersion, and anisotropy (124–134). These ultrasound techniques have the advantage of being very rapid and allowing significant flexibility in how they can interrogate the muscle. However, they are also limited in that they are not able to measure the full 3D vector motion of the tissue.

Early work in the study of skeletal muscle with MRE showed a linear relationship between muscle stiffness and muscle tension in muscles undergoing passive and active contractions (135) (Figure 5), variations in stiffness between different muscles (136,137), and anisotropic stiffness in ex vivo bovine muscle tissue (44). In a study involving 8 control subjects and 6 subjects with various lower-extremity neuromuscular dysfunctions (paraplegia with spasticity, paraplegia with flaccidity, and poliomyelitis), MRE determined that the relaxed muscle stiffnesses of the tibialis anterior, medial and lateral gastrocnemius, and soleus of the subjects with impaired neuromuscular systems were significantly higher than for the control subjects (138). Investigations of the viscoelastic properties of skeletal muscle showed that in a study involving 9 patients with active myositis and 9 age- and gender-matched controls, the stiffness of the vastus medialis was lower in the patients with myositis than in the healthy controls (139), and that in a study of the shear wave attenuation coefficient for 14 control subjects, 6 subjects with myositis, and 7 subjects with hyperthyroid myopathy, the attenuation was found to be larger in the diseased muscles than it was in healthy muscle (140). Furthermore, it was reported that in the 4 hyperthyroid patients who were retested, the mean attenuation coefficient of these patients decreased posttreatment to values closer to that of healthy muscle. In a study of 5 hyperthyroid patients imaged before and after treatment and 5 control subjects, the stiffness of the relaxed vastus medialis muscle in the patients examined before treatment was lower than for the healthy controls, and their mean

muscle stiffness increased to within the range of the healthy subjects after treatment (141). In a preliminary report focused on the study of myofascial pain and fibromyalgia, the stiffness of the upper-trapezial taut band in 4 women with myofasical pain was determined to be higher than in the region surrounding the taut bands, the unaffected contralateral trapezious muscle, and the mean value from a cohort of 4 healthy control subjects (142), a finding in agreement with a recent study involving vibration sonoelastography to assess myofasical trigger points (129).

Recent developments in the area of muscle MRE have also included a number of technical developments that may eventually provide clinical utility in the future. In one such study, MRE of the tongue and soft palate was performed in 7 healthy volunteers (mean age: 25.4 years) (143). Motion was produced at 80 Hz via electromechanical voice coils attached to a bite bar equipped with a custom-fit mouth guard. The results of their study indicated that at 80 Hz, the mean stiffness of the tongue and soft palate for their subjects was similar (storage modulus: 2.67 ± 0.29 and 2.53 ± 0.31 kPa, respectively; loss modulus: 0.85 ± 0.07 kPa and 0.90 ± 0.22 kPa, respectively). A preliminary follow-up study involving 5 patients with severe obstructive sleep apnea (OSA) and 5 normal subjects indicated that the storage and loss moduli of the tongue are lower in OSA patients (storage modulus: 1.47 ± 0.97 vs. 2.72 ± 0.40 kPa, $p<0.05$; loss modulus: 0.54 ± 0.31 vs. 1.03 ± 0.14 kPa, $p<0.05$) whereas the properties of the soft palate were not significantly different (storage modulus: 1.59 ± 0.92 vs. 2.12 ± 0.91 kPa, $p>0.05$; loss modulus: 0.49 ± 0.29 vs. 0.15 ± 0.48 kPa, $p>0.05$) (144). In other studies, the in vivo anisotropic properties of skeletal muscle have been explored with MRE which may provide a more accurate description of muscle mechanical properties, and thus better metrics to gauge the changes in muscle due to various diseases. In one study of the biceps of 5 healthy volunteers, a transversely isotropic elasticity model was used to estimate the perpendicular and parallel shear moduli of the biceps to be 5.5 ± 0.9 kPa and 29.3 ± 6.2 kPa, respectively (145). In a more recent study by the same authors, their model of the anisotropic properties of muscle was used to design a multifrequency MRE acquisition for measuring the parallel shear modulus of the femoral muscles (146). They collected data at 4 frequencies of motion (25–62.5 Hz) in 7 volunteers while relaxed and during isometric contraction of the muscles. The complex shear moduli were then fit to a spring-pot viscoelastic model. The results indicated that the muscle elasticity and structure parameters both changed from the relaxed to the contracted state (2.68 ± 0.23 to 3.87 ± 0.50 kPa and 0.253 ± 0.009 to 0.270 ± 0.009, respectively).

An example of an alternative application of MRE that can use techniques similar to muscle MRE is imaging the stiffness of the plantar fat pads of diabetic patients (147). In this study of 12 normal volunteers and 4 patients with diabetes imaged with 3D MRE and inverted using a finite-element technique, the heel fat pads of the patients were found to be stiffer than those of the normal volunteers (5.26 ± 0.56 kPa vs. 4.85 ± 0.56 kPa). MRE motion-encoding techniques have also been employed to develop the means to examine the connectivity of adjacent tissues. One initial investigation focused on looking at the scattering properties of shear waves across material boundaries to glean information about the degree of connectivity at the boundary (148). Another study looked at visualizing the presence of slip interfaces between tissues (i.e., regions in which adjacent tissues are free to slide past each other rather than being fixed to each other) using the differential amounts of motion occurring on either side of tissue boundaries to produce intravoxel signal attenuation at the boundaries (149). In this latter work, examples were shown of imaging the boundary between the peritoneal wall and small bowel, the transversus abdominus and oblique muscles, and between the functional compartments of the forearm flexor and extensor muscles. One of the potential uses for these techniques would be for the visualization of abdominal adhesions which can develop after surgery and cause significant health problems. In another application, a technique for imaging the functional components of the extrinsic

flexor muscles of the forearm (regions that are indistinct anatomically but have selective functional activation) was demonstrated in which individual fingers were selectively vibrated to produce localized motion within the associated flexor muscles (150). This technique could help to identify these regions of the muscles for anatomic and physiology studies, for example, which require placing electromyography probes and quantifying tendon excursions.

MRE OF THE BRAIN

Another promising recent development for MRE is for the assessment of the mechanical properties of the tissues of the central nervous system (CNS), specifically the brain (151). Knowledge about brain tissue mechanical properties is important for understanding the mechanics of brain injury, development, and pathophysiology and could provide insight into a myriad of conditions. While, conventional MRI has provided significant contributions for the evaluation of diseases such as multiple sclerosis (MS) and Alzheimer's disease (AD) (152–156), our understanding of these conditions could be improved given more information about the mechanical changes of the tissue that accompany the neurodegeneration, demyelination, or plaque and tangle development that occurs during the onset and progression of these diseases. Similarly, MRI has demonstrated great success in classifying brain neoplasms and imaging their structure and that of the surrounding anatomy (157–159). However, more information is still necessary to guide physicians in the pre- and post-treatment management of these tumors (160). Measuring and monitoring the mechanical properties of tumors and the surrounding brain tissue could provide valuable information about the tumors and their response to treatment. In the case of a condition like hydrocephalus, the visible abnormal changes in the tissue can be caused by changes in the mechanical properties of the brain, such as the ventricular compliance (161); changes which may be discernable with a technique capable of measuring brain tissue stiffness.

The brain is protected and isolated by the cranium, so little is known about the in vivo quantitative mechanical characteristics of healthy brain tissue and how these properties change due to different diseases. A significant amount of work has been done on ex vivo specimens and in animal models (including MRE studies of mouse, rat, feline, and porcine brain tissue (43,162–165)), but the in vivo properties of human brain tissue are still a mystery. Because ultrasound does not transmit easily through the skull, in vivo ultrasound elasticity imaging of the brain is currently limited to intraoperative procedures (166). As summarized by several authors, studies of the biomechanical properties of brain tissue have involved significant variations in tissue type, animal species, and experimental conditions, which makes comparing results from different studies challenging (167–169). These results have led to significant variations in the reported stiffness of brain tissue, and even conflicting reports as to whether white matter is stiffer or softer than gray matter. Many of the techniques researchers have used to study brain tissue properties have required either in vitro or invasive analysis. MRE, on the other hand, offers a unique opportunity to study these properties in vivo and noninvasively. Preliminary work with MRE has produced measurements of healthy brain tissue properties using several different approaches as well as assessments of changes in brain tissue properties due to AD, MS, normal-pressure hydrocephalus, and cancer.

In a study by Kruse et al. involving 25 healthy subjects ranging from 23 to 79 years of age using 100-Hz mechanical vibrations and a 2D inversion of the MRE wave data, the stiffness of white matter was determined to be significantly larger than for gray matter (13.6 kPa vs. 5.22 kPa, $p < 0.0001$) and no significant variation in brain stiffness with age was observed (168). Green et al. found in an investigation involving 5 healthy subjects imaged with a 3D MRE protocol using 90-Hz vibrations that gray matter was stiffer than white matter (3.1 kPa

vs. 2.7 kPa, p = 0.02) (170). Using a similar technique with 80-Hz vibrations, it was shown that the stiffness of the cerebellum in normal subjects is significantly lower than the stiffness of the cerebrum (storage modulus: 1.72 ± 0.15 vs. 2.22 ± 0.28 kPa, p<0.001; loss modulus: 0.95 ± .14 vs. 0.99 ± 0.25 kPa, p>0.4) (171). In a larger study involving 55 healthy subjects (23 females and 32 males of various ages), a multifrequency MRE technique was used to measure the complex shear modulus at frequencies from 25 to 62.5 Hz (Figure 6), which was then fit to a spring-pot viscoelastic model. By treating the various brain tissues as having the same material properties, Sack et al. detected that the viscoelastic parameter in their model declined with age at a rate of about 0.8% per year (p<0.001) (172) (Figure 7). Furthermore, they found that the brain stiffness of their female subjects was elevated compared to their age-matched male counterparts. In a follow-up study involving 45 MS patients with mild relapsing-remitting disease course and 34 age- and gender-matched control subjects, a similar difference was found between the brain stiffness of their male and female subjects, and they also found that the brain tissue in the MS patients was significantly softer (by about 13%) than in the healthy subjects (173). In another follow-up study, 17 MS patients and 42 age- and gender-matched control subjects were studied to assess the effect of MS on brain stiffness and volume. The observed decrease in stiffness for the MS patients compared to the healthy subjects (17%) was a significant predictor of the disease (p < 0.0001) whereas the decrease in total brain volume (5%) due to demyelination and neuronal degradation was not significant (p = 0.021) (174). This same methodology has also been applied recently to the study of normal-pressure hydrocephalus (NPH) (46,175). In those studies, multifrequency MRE was performed on 20 patients (8 male, 12 female) with primary (n=14) and secondary (n=6) NPH (mean age: 71 years) before and after shunt placement and 25 healthy volunteers (10 male, 15 female; mean age: 62.1). The results showed that the brain tissue of the NPH subjects was about 25% softer than for the healthy subjects (p < 0.001) and that the tissue structure parameter in their model was about 10% lower in the NPH subjects (p < 0.001). 3 months post-treatment, the pre- and post-shunt brain stiffnesses were not significantly different. However, the tissue structure parameter increased post-shunt and was not significantly different from the value for the control subjects. In a preliminary study of 7 patients with probable AD, 14 age- and gender-matched PIB- cognitively normal controls, and 7 age- and gender-matched PIB+ cognitively normal controls (PIB being an amyloid PET tracer indicating the presence of β-amyloid, a hallmark of AD), the median brain stiffness of the AD group was significantly lower than for the cognitively normal groups, and the cognitively normal groups were not significantly different from each other (176). All of these results suggest that MRE may be a useful tool for studying diffuse changes in brain tissue mechanics due a number of diseases.

Preliminary reports of the application of MRE for studying focal brain diseases have included studies of tumors and response to stroke. In one study of the mechanical properties of brain tumors, 6 patients with 6 known tumors were imaged with MRE and the relative stiffness of the tumors with respect to the white matter in each subject was compared to the neurosurgeon’s report of the tumor consistency after surgical resection (177). The MRE and intraoperative assessments of tumor stiffness agreed with each other in all cases. Specifically, 1 transitional meningioma was found to be soft, 2 fibrous meningiomas were found to have intermediate stiffness, and the other 3 lesions were found to be stiff (a shwannoma, a hemangiopericytoma, and a transitional meningioma). In a feasibility study investigating the use of MRE for assessing the impact a stroke has on brain tissue mechanical properties, multifrequency MRE was performed on a patient 4 days after a left/right middle cerebral artery (MCA) territory infarction (178). In this subject, both the storage and loss shear moduli (i.e., stiffness) at each frequency were lower in the stroke region than they were in the unaffected parenchyma.

One of the primary challenges with conventional dynamic MRE for brain imaging is introducing the mechanical vibrations into the brain. A number of techniques have been developed over the years to do this, including bite bars, actuators placed under the head, and devices that vibrate a holder the head rests in (10,16,168,170,172,179). To further improve patient comfort and to reduce the complexity of brain MRE hardware, researchers have pursued alternative ways of producing the brain tissue motion necessary for MRE. In one early study, a subject was asked to hum during an MRE scan and a nasal cannula connected to a microphone was used to detect the pitch of the vocalization and that measured waveform was used in a feedback circuit to produce matched motion-encoding gradients in a local gradient coil (180). Motion throughout the brain was readily visible due to this intrinsic source of vibration. In a different study, vibrations transferred to the brain due to the vibration of the scanner table produced by the application of large gradients in the imaging sequence, such as those normally used for diffusion-weighted imaging, were used to estimate gray matter and white matter stiffness in a healthy volunteer (5–10 kPa and 15–30 kPa, respectively) (181). A number of other methods have been used to image the intrinsic motion of the brain that occurs due to vascular and CSF pulsation during the cardiac cycle to provide a means for assessing brain motion and brain tissue mechanical properties (182–186). In one such study, a cardiac-gated velocity-encoding imaging sequence (VENC = 1 cm/sec) was used to image this intrinsic motion of the brain in 5 healthy volunteers (183). The resulting displacement fields were fit to a basic damped wave propagation model to determine the wave propagation speed in the tissue and thus the tissue stiffness and they obtained a mean stiffness of 4.7± 3.6 kPa for the 5 volunteers. In another study, a cine DENSE EPI acquisition was used to measure this pulsatile motion in a patient with a meningioma (184). The displacement data were used to calculate the internal strains occurring in the tissue and showed that the tumor could be distinguished as a region with lower strain than the surrounding brain tissue, indicative of the tumor being stiffer than the adjacent tissue.

CARDIAC MRE

Significant work has been done over the years to understand and model the mechanical function of the heart. Cardiac disease is a primary cause of death in the United States and conditions like diastolic dysfunction and hypertension can cause and be caused by changes in the mechanical properties of cardiac tissues (187,188). The current gold standard for the assessment of cardiac mechanical properties comes from the use of pressure and volume measurements of the heart during the cardiac cycle (189). This information can be used to derive global estimates of the properties of the left ventricular myocardium. Several ultrasound and MRI techniques have been developed to directly image the motion of cardiac tissue and to use that information to assess heart function and to calculate relative measures of tissue mechanical properties (e.g., strain) (190–196). The application of these techniques is somewhat limited since these relative values are not comparable between individuals, and some of these techniques only yield global estimates of tissue properties, which may not be useful for studying localized pathologies like infarcts. Other work has focused on developing high-frame-rate ultrasound imaging systems capable of imaging the rapid, transient, intrinsic mechanical vibrations within the heart during the cardiac cycle and using that information to calculate quantitative mechanical properties of cardiac tissues (197–199).

While work has been done to develop some of these qualitative MR techniques into quantitative ones (e.g., (200)), several quantitative and qualitative MRE techniques are being evaluated for use in studying cardiac tissue mechanical properties as well. In one implementation of cardiac MRE, wave propagation in the interventricular septum (IVS) due to 48.5-Hz mechanical vibrations applied to the chest wall was imaged with a bSSFP MRE acquisition (201). In their volunteer, the average shear wave speed over the cardiac cycle

was 2.5 m/s (i.e., a shear stiffness of about 6.25 kPa). In a different form of cardiac MRE, shear wave amplitude variations throughout the heart during the cardiac cycle are used to provide relative measures of tissue stiffness and ventricular pressure (202–206). In this application, mechanical vibrations at 24.3 Hz are applied to the chest wall and the resulting wave propagation in the heart is measured in the left ventricle with a cine GRE MRE acquisition. In one report, the shear wave amplitude was about 2.45 times higher in the left ventricle in diastole than in systole in their 6 healthy volunteers, which their model predicted corresponded to about a 36-fold-higher stiffness of the myocardium in systole compared to diastole (202). This information can also be used to estimate left ventricular pressure during the cardiac cycle and may be useful as a surrogate to invasive pressure measurements for the construction of the pressure-volume (P-V) loops often studied in cardiac MR (203). In a follow-up study of 11 young healthy subjects, 5 older healthy subjects, and 11 subjects with echocardiographically proven relaxation abnormalities (mean age: 31.7, 54.8, and 58 years, respectively), the mean wave amplitude in the left ventricle and the mean ratio of the wave amplitude in the left ventricle to the amplitude in the anterior chest wall were both significantly lower in the patient population than in the healthy subjects (205). This suggests that it may be possible to use MRE to diagnose patients with myocardial relaxation abnormalities. In a preliminary animal study of 3 pigs comparing wave-amplitude MRE and invasive ventricular pressure measurements, a significant correlation between the two measurements was found which further supports the idea that MRE can be used as a tool for noninvasively assessing the mechanics of the left ventricle (204).

In two other cardiac MRE methods, shear wave displacement fields measured in the heart are inverted to provide quantitative estimates of tissue stiffness throughout the cardiac cycle. In one of these studies, the authors demonstrated a cine GRE technique for performing MRE in vivo and measured the myocardial stiffness in 5 healthy volunteers and found that the stiffness varied from 6.5–8.7 kPa in diastole to 8.3–11.3 kPa in systole (207) (Figure 8). In other studies by the same authors, the technique was used to collect displacement information during the cardiac cycle which was used to derive stiffness estimates of the myocardium that were shown to correlate with invasive measurements of the left ventricular pressure and standard P-V loops in a study of 6 healthy pigs (208) (Figure 9) and end-diastolic left-ventricular pressure was found to correlate with stiffness in a study to 4 pigs infused with Dextran-40 to assess cardiac tissue stiffness changes with pressure with minimal effects due to active contraction (209). In these current studies, the direct relationship between myocardial stiffness and ventricular pressure varies significantly from subject to subject, so determining a single relationship between the two that will allow stiffness measurements to replace pressure measurements is an ongoing area of research. In the other direct-inversion MRE technique, a DENSE MRE imaging sequence was demonstrated using 2 healthy volunteers to measure displacement and stiffness changes at various points in the cardiac cycle (210,211). In that study, myocardial stiffness increased from about 10 kPa in diastole to about 25 kPa in systole. So far, the in vivo applications of MRE for assessing cardiac mechanical properties are preliminary, but the prospect of determining ventricular pressure, myocardial stiffness, and cardiac dysfunction information in vivo noninvasively is exciting.

SUMMARY

This review has highlighted a number of existing and emerging applications for MR elastography. These have included techniques to (1) replace the need for invasive procedures like biopsies and ventricular pressure readings, (2) provide supplemental information about tissue properties to improve disease diagnosis, and (3) change our understanding of the pathobiology of certain diseases. The future will offer significant developments in terms of

both the technology for performing MRE, as well as the breadth of clinical applications for which it is used.

Acknowledgments

Grant Support: NIH EB001981

References

1. American Cancer Society. Cancer facts & figures. Atlanta, GA: American Cancer Society, Inc; 2008. p. 70
2. Fatemi M, Manduca A, Greenleaf JF. Imaging elastic properties of biological tissues by low-frequency harmonic vibration. Proc IEEE. 2003; 91:1503–1519.
3. Greenleaf JF, Fatemi M, Insana M. Selected methods for imaging elastic properties of biological tissues. Annu Rev Biomed Eng. 2003; 5:57–78. [PubMed: 12704084]
4. Parker KJ, Doyley MM, Rubens DJ. Imaging the elastic properties of tissue: the 20 year perspective. Phys Med Biol. 2011; 56:R1–R29. [PubMed: 21119234]
5. Chenevert TL, Skovoroda AR, O'Donnell M, Emelianov SY. Elasticity reconstructive imaging by means of stimulated echo MRI. Magnet Reson Med. 1998; 39:482–490.
6. Steele DD, Chenevert TL, Skovoroda AR, Emelianov SY. Three-dimensional static displacement, stimulated echo NMR elasticity imaging. Physics in Medicine and Biology. 2000; 45:1633–1648. [PubMed: 10870715]
7. Lewa CJ, de Certaines JD. MR imaging of viscoelastic properties. J Magn Reson Imaging. 1995; 5:242–244. [PubMed: 7766988]
8. Lewa CJ, De Certaines JD. Viscoelastic property detection by elastic displacement NMR measurements. J Magn Reson Imaging. 1996; 6:652–656. [PubMed: 8835959]
9. Lewa CJ, Roth M, Nicol L, Franconi JM, de Certaines JD. A new fast and unsynchronized method for MRI of viscoelastic properties of soft tissues. J Magn Reson Imaging. 2000; 12:784–789. [PubMed: 11050651]
10. Sabet AA, Christoforou E, Zatlin B, Genin GM, Bayly PV. Deformation of the human brain induced by mild angular head acceleration. J Biomech. 2008; 41:307–315. [PubMed: 17961577]
11. Muthupillai R, Lomas DJ, Rossman PJ, Greenleaf JF, Manduca A, Ehman RL. Magnetic resonance elastography by direct visualization of propagating acoustic strain waves. Science. 1995; 269:1854–1857. [PubMed: 7569924]
12. Muthupillai R, Ehman RL. Magnetic resonance elastography. Nat Med. 1996; 2:601–603. [PubMed: 8616724]
13. Axel L. Biomechanical dynamics of the heart with MRI. Annu Rev Biomed Eng. 2002; 4:321–347. [PubMed: 12117761]
14. Plewes DB, Betty I, Urchuk SN, Soutar I. Visualizing tissue compliance with MR imaging. J Magn Reson Imaging. 1995; 5:733–738. [PubMed: 8748495]
15. Uffmann K, Ladd ME. Actuation systems for MR elastography: design and applications. IEEE Eng Med Biol Mag. 2008; 27:28–34. [PubMed: 18519179]
16. Tse ZT, Janssen H, Hamed A, Ristic M, Young I, Lamperth M. Magnetic resonance elastography hardware design: a survey. Proc Inst Mech Eng H. 2009; 223:497–514. [PubMed: 19499839]
17. Manduca A, Oliphant TE, Dresner MA, et al. Magnetic resonance elastography: non-invasive mapping of tissue elasticity. Med Image Anal. 2001; 5:237–254. [PubMed: 11731304]
18. Manduca A, Lake DS, Kruse SA, Ehman RL. Spatio-temporal directional filtering for improved inversion of MR elastography images. Med Image Anal. 2003; 7:465–473. [PubMed: 14561551]
19. McCracken PJ, Manduca A, Felmlee J, Ehman RL. Mechanical transient-based magnetic resonance elastography. Magn Reson Med. 2005; 53:628–639. [PubMed: 15723406]
20. Oliphant TE, Manduca A, Ehman RL, Greenleaf JF. Complex-valued stiffness reconstruction for magnetic resonance elastography by algebraic inversion of the differential equation. Magn Reson Med. 2001; 45:299–310. [PubMed: 11180438]

21. Yin M, Woollard J, Wang X, et al. Quantitative assessment of hepatic fibrosis in an animal model with magnetic resonance elastography. Magn Reson Med. 2007; 58:346–353. [PubMed: 17654577]
22. Romano AJ, Shirron JJ, Bucaro JA. On the noninvasive determination of material parameters from a knowledge of elastic displacements: Theory and numerical simulation. Ieee T Ultrason Ferr. 1998; 45:751–759.
23. Romano AJ, Bucaro JA, Ehman RL, Shirron JJ. Evaluation of a material parameter extraction algorithm using MRI-based displacement measurement. Ieee T Ultrason Ferr. 2000; 47:1575–1581.
24. Romano AJ, Abraham PB, Rossman PJ, Bucaro JA, Ehman RL. Determination and analysis of guided wave propagation using magnetic resonance elastography. Magn Reson Med. 2005; 54:893–900. [PubMed: 16155879]
25. Perrinez PR, Kennedy FE, Van Houten EE, Weaver JB, Paulsen KD. Magnetic resonance poroelastography: an algorithm for estimating the mechanical properties of fluid-saturated soft tissues. IEEE Trans Med Imaging. 2010; 29:746–755. [PubMed: 20199912]
26. Klatt D, Hamhaber U, Asbach P, Braun J, Sack I. Noninvasive assessment of the rheological behavior of human organs using multifrequency MR elastography: a study of brain and liver viscoelasticity. Phys Med Biol. 2007; 52:7281–7294. [PubMed: 18065839]
27. Sinkus R, Lorenzen J, Schrader D, Lorenzen M, Dargatz M, Holz D. High-resolution tensor MR elastography for breast tumour detection. Phys Med Biol. 2000; 45:1649–1664. [PubMed: 10870716]
28. Sinkus R, Siegmann K, Xydeas T, Tanter M, Claussen C, Fink M. MR elastography of breast lesions: understanding the solid/liquid duality can improve the specificity of contrast-enhanced MR mammography. Magn Reson Med. 2007; 58:1135–1144. [PubMed: 17969009]
29. Lee TH, Ahn CY, Kwon OI, Seo JK. A hybrid one-step inversion method for shear modulus imaging using time-harmonic vibrations. Inverse Probl. 2010; 26:13.
30. Van Houten EE, Miga MI, Weaver JB, Kennedy FE, Paulsen KD. Three-dimensional subzone-based reconstruction algorithm for MR elastography. Magn Reson Med. 2001; 45:827–837. [PubMed: 11323809]
31. Sinkus R, Tanter M, Xydeas T, Catheline S, Bercoff J, Fink M. Viscoelastic shear properties of in vivo breast lesions measured by MR elastography. Magn Reson Imaging. 2005; 23:159–165. [PubMed: 15833607]
32. Suki B, Barabasi AL, Lutchen KR. Lung tissue viscoelasticity: a mathematical framework and its molecular basis. J Appl Physiol. 1994; 76:2749–2759. [PubMed: 7928910]
33. Doyley MM, Perreard I, Patterson AJ, Weaver JB, Paulsen KM. The performance of steady-state harmonic magnetic resonance elastography when applied to viscoelastic materials. Med Phys. 2010; 37:3970–3979. [PubMed: 20879559]
34. Bishop J, Samani A, Sciarretta J, Plewes DB. Two-dimensional MR elastography with linear inversion reconstruction: methodology and noise analysis. Phys Med Biol. 2000; 45:2081–2091. [PubMed: 10958181]
35. Van Houten EEW, Viviers DV, McGarry MDJ, et al. Subzone based magnetic resonance elastography using a Rayleigh damped material model. Medical Physics. 2011; 38:1993–2004. [PubMed: 21626932]
36. Oestreicher HL. Field and impedance of an oscillating sphere in a viscoelastic medium with application to biophysics. The Journal of the Acoustical Society of America. 1951; 23:707–714.
37. Christensen, RM. Theory of viscoelasticity. 2. Mineola, NY: Dover Publications; 2003. p. 364
38. Sarvazyan, AP.; Skovoroda, AR.; Emelianov, SY., et al. Biophysical Bases of Elasticity Imaging. In: Jones, JP., editor. Acoustical Imaging. Vol. 21. New York: Plenum Press; 1995. p. 223-240.
39. Duck, FA. Physical properties of tissue: a comprehensive reference book. London: Academic Press; 1990. p. 346
40. Sinkus R, Daire JL, Van Beers BE, Vilgrain V. Elasticity reconstruction: beyond the assumption of local homogeneity. C R Mecanique. 2010; 338:474–479.
41. Auld, BA. Acoustic fields and waves in solids. 2. Malabar, FL: R.E. Krieger; 1990. p. 435

42. Holm S, Sinkus R. A unifying fractional wave equation for compressional and shear waves. J Acoust Soc Am. 2010; 127:542–559. [PubMed: 20058999]
43. Clayton EH, Garbow JR, Bayly PV. Frequency-dependent viscoelastic parameters of mouse brain tissue estimated by MR elastography. Phys Med Biol. 2011; 56:2391–2406. [PubMed: 21427486]
44. Kruse SA, Smith JA, Lawrence AJ, et al. Tissue characterization using magnetic resonance elastography: preliminary results. Phys Med Biol. 2000; 45:1579–1590. [PubMed: 10870712]
45. Riek K, Klatt D, Nuzha H, et al. Wide-range dynamic magnetic resonance elastography. J Biomech. 2011; 44:1380–1386. [PubMed: 21295305]
46. Streitberger KJ, Wiener E, Hoffmann J, et al. In vivo viscoelastic properties of the brain in normal pressure hydrocephalus. NMR Biomed. 2011; 24:385–392. [PubMed: 20931563]
47. Asbach P, Klatt D, Schlosser B, et al. Viscoelasticity-based staging of hepatic fibrosis with multifrequency MR elastography. Radiology. 2010; 257:80–86. [PubMed: 20679447]
48. Bataller R, Brenner DA. Liver fibrosis. J Clin Invest. 2005; 115:209–218. [PubMed: 15690074]
49. Tsukada S, Parsons CJ, Rippe RA. Mechanisms of liver fibrosis. Clin Chim Acta. 2006; 364:33–60. [PubMed: 16139830]
50. Friedman SL. Liver fibrosis -- from bench to bedside. J Hepatol. 2003; 38 (Suppl 1):S38–53. [PubMed: 12591185]
51. Poynard T, McHutchison J, Manns M, et al. Impact of pegylated interferon alfa-2b and ribavirin on liver fibrosis in patients with chronic hepatitis C. Gastroenterology. 2002; 122:1303–1313. [PubMed: 11984517]
52. Dixon JB, Bhathal PS, Hughes NR, O'Brien PE. Nonalcoholic fatty liver disease: improvement in liver histological analysis with weight loss. Hepatology. 2004; 39:1647–1654. [PubMed: 15185306]
53. Thampanitchawong P, Piratvisuth T. Liver biopsy: complications and risk factors. World J Gastroenterol. 1999; 5:301–304. [PubMed: 11819452]
54. Regev A, Berho M, Jeffers LJ, et al. Sampling error and intraobserver variation in liver biopsy in patients with chronic HCV infection. Am J Gastroenterol. 2002; 97:2614–2618. [PubMed: 12385448]
55. Bonekamp S, Kamel I, Solga S, Clark J. Can imaging modalities diagnose and stage hepatic fibrosis and cirrhosis accurately? J Hepatol. 2009; 50:17–35. [PubMed: 19022517]
56. Talwalkar JA, Yin M, Fidler JL, Sanderson SO, Kamath PS, Ehman RL. Magnetic resonance imaging of hepatic fibrosis: emerging clinical applications. Hepatology. 2008; 47:332–342. [PubMed: 18161879]
57. Sandrin L, Fourquet B, Hasquenoph JM, et al. Transient elastography: a new noninvasive method for assessment of hepatic fibrosis. Ultrasound Med Biol. 2003; 29:1705–1713. [PubMed: 14698338]
58. Cohen EB, Afdhal NH. Ultrasound-based hepatic elastography: origins, limitations, and applications. J Clin Gastroenterol. 2010; 44:637–645. [PubMed: 20844365]
59. Stebbing J, Farouk L, Panos G, et al. A meta-analysis of transient elastography for the detection of hepatic fibrosis. J Clin Gastroenterol. 2010; 44:214–219. [PubMed: 19745758]
60. Andersen ES, Christensen PB, Weis N. Transient elastography for liver fibrosis diagnosis. Eur J Intern Med. 2009; 20:339–342. [PubMed: 19524169]
61. Castera L, Foucher J, Bernard PH, et al. Pitfalls of liver stiffness measurement: a 5-year prospective study of 13,369 examinations. Hepatology. 2010; 51:828–835. [PubMed: 20063276]
62. Salameh N, Peeters F, Sinkus R, et al. Hepatic viscoelastic parameters measured with MR elastography: correlations with quantitative analysis of liver fibrosis in the rat. J Magn Reson Imaging. 2007; 26:956–962. [PubMed: 17896384]
63. Salameh, N.; Larrat, B.; Abarca-Quinones, J.; Leclercq, I.; Sinkus, R.; Van Beers, BE. MR elastography of non-alcoholic steatohepatitis in the rat. Proceedings of the 16th Annual Meeting of ISMRM; Toronto, Ontario, Canada. 2008. p. 85
64. Salameh, N.; Larrat, B.; Abarca-Quinones, J., et al. MR elastography for the early detection of steatohepatitis in the rat with fatty liver. Proceedings of the 17th Annual Meeting of ISMRM; Honolulu, HI. 2009. p. 4090

65. Huwart L, Sempoux C, Vicaut E, et al. Magnetic resonance elastography for the noninvasive staging of liver fibrosis. Gastroenterology. 2008; 135:32–40. [PubMed: 18471441]
66. Yin M, Talwalkar JA, Glaser KJ, et al. Assessment of hepatic fibrosis with magnetic resonance elastography. Clin Gastroenterol Hepatol. 2007; 5:1207–1213. [PubMed: 17916548]
67. Bensamoun SF, Wang L, Robert L, Charleux F, Latrive JP, Ho Ba Tho MC. Measurement of liver stiffness with two imaging techniques: magnetic resonance elastography and ultrasound elastometry. J Magn Reson Imaging. 2008; 28:1287–1292. [PubMed: 18972339]
68. Rouviere O, Yin M, Dresner MA, et al. MR elastography of the liver: preliminary results. Radiology. 2006; 240:440–448. [PubMed: 16864671]
69. Huwart L, Peeters F, Sinkus R, et al. Liver fibrosis: non-invasive assessment with MR elastography. NMR Biomed. 2006; 19:173–179. [PubMed: 16521091]
70. Asbach P, Klatt D, Hamhaber U, et al. Assessment of liver viscoelasticity using multifrequency MR elastography. Magn Reson Med. 2008; 60:373–379. [PubMed: 18666132]
71. Hines CD, Bley TA, Lindstrom MJ, Reeder SB. Repeatability of magnetic resonance elastography for quantification of hepatic stiffness. J Magn Reson Imaging. 2010; 31:725–731. [PubMed: 20187219]
72. Motosugi U, Ichikawa T, Sano K, et al. Magnetic resonance elastography of the liver: preliminary results and estimation of inter-rater reliability. Jpn J Radiol. 2010; 28:623–627. [PubMed: 20972864]
73. Wang Y, Ganger DR, Levitsky J, et al. Assessment of chronic hepatitis and fibrosis: comparison of MR elastography and diffusion-weighted imaging. AJR Am J Roentgenol. 2011; 196:553–561. [PubMed: 21343496]
74. Venkatesh, SK.; Tai, D.; Wee, A.; Xu, S.; Yu, H. Comparison of liver stiffness with MRE and fibrosis quantification with Fibro-C index in chronic hepatitis B patients. Proceedings of the 19th Annual Meeting of ISMRM; Montreal, Quebec, Canada. 2011. p. 2934
75. Seitz M, Reichenbach S, Moller B, Zwahlen M, Villiger PM, Dufour JF. Hepatoprotective effect of tumour necrosis factor {alpha} blockade in psoriatic arthritis: a cross-sectional study. Ann Rheum Dis. 2010; 69:1148–1150. [PubMed: 19854710]
76. Chen, J.; Hoganson, D.; Yin, M., et al. Estimation of the prevalence of liver fibrosis in patients receiving chronic methotrexate therapy with MR elastography. Proceedings of the 18th Annual Meeting of ISMRM; Stockholm, Sweden. 2010. p. 4633
77. Laharie D, Seneschal J, Schaeverbeke T, et al. Assessment of liver fibrosis with transient elastography and FibroTest in patients treated with methotrexate for chronic inflammatory diseases: a case-control study. J Hepatol. 2010; 53:1035–1040. [PubMed: 20801541]
78. Watanabe H, Kanematsu M, Kitagawa T, et al. MR elastography of the liver at 3 T with cine-tagging and bending energy analysis: preliminary results. Eur Radiol. 2010; 20:2381–2389. [PubMed: 20440504]
79. Mannelli, L.; Kolokythas, O.; Dubinsky, TJ.; Gunn, M.; Potter, CA.; Maki, JH. Tag MRI of the liver as a new method to differentiate normal vs. cirrhotic livers. Proceedings of the 19th Annual Meeting of ISMRM; Montreal, Quebec, Canada. 2011. p. 2937
80. Chung, S.; Breton, E.; Mannelli, L.; Axel, L. Liver stiffness assessment by tagged MRI of cardiac-induced liver motion. Proceedings of the 19th Annual Meeting of ISMRM; Montreal, Quebec, Canada. 2011. p. 2935
81. Lupsor M, Badea R, Stefanescu H, et al. Performance of unidimensional transient elastography in staging non-alcoholic steatohepatitis. J Gastrointestin Liver Dis. 2010; 19:53–60. [PubMed: 20361076]
82. Chan HL, Wong GL, Choi PC, et al. Alanine aminotransferase-based algorithms of liver stiffness measurement by transient elastography (Fibroscan) for liver fibrosis in chronic hepatitis B. J Viral Hepat. 2009; 16:36–44. [PubMed: 18673426]
83. Fraquelli M, Rigamonti C, Casazza G, et al. Reproducibility of transient elastography in the evaluation of liver fibrosis in patients with chronic liver disease. Gut. 2007; 56:968–973. [PubMed: 17255218]
84. Yashima Y, Tsujino T, Masuzaki R, et al. Increased liver elasticity in patients with biliary obstruction. J Gastroenterol. 2011; 46:86–91. [PubMed: 20814804]

85. Salameh N, Larrat B, Abarca-Quinones J, et al. Early detection of steatohepatitis in fatty rat liver by using MR elastography. Radiology. 2009; 253:90–97. [PubMed: 19587308]
86. Wang, Y.; Miller, FH.; McCarthy, R., et al. Chronic hepatitis and fibrosis assessed by magnetic resonance elastography (MRE). Proceedings of the 18th Annual Meeting of ISMRM; Stockholm, Sweden. 2010. p. 4636
87. Hu, T.; Silva, A.; Hu, L.; Ehman, R. Utilizing magnetic resonance elastography in the evaluation of liver donors. Proceedings of the 18th Annual Meeting of ISMRM; Stockholm, Sweden. 2010. p. 4655
88. Chen J, Talwalkar JA, Yin M, Glaser KJ, Sanderson SO, Ehman RL. Early detection of nonalcoholic steatohepatitis in patients with nonalcoholic fatty liver disease by using MR elastography. Radiology. 201110.1148/radiol.11101942
89. Lupsor M, Badea R, Stefanescu H, et al. Performance of a new elastographic method (ARFI technology) compared to unidimensional transient elastography in the noninvasive assessment of chronic hepatitis C. Preliminary results. J Gastrointestin Liver Dis. 2009; 18:303–310. [PubMed: 19795024]
90. Arena U, Vizzutti F, Abraldes JG, et al. Reliability of transient elastography for the diagnosis of advanced fibrosis in chronic hepatitis C. Gut. 2008; 57:1288–1293. [PubMed: 18448567]
91. Mendizabal M, Reddy KR. Current management of hepatocellular carcinoma. Med Clin North Am. 2009; 93:885–900. [PubMed: 19577120]
92. Dong MH, Saab S. Complications of cirrhosis. Dis Mon. 2008; 54:445–456. [PubMed: 18570914]
93. Venkatesh SK, Yin M, Glockner JF, et al. MR elastography of liver tumors: preliminary results. AJR Am J Roentgenol. 2008; 190:1534–1540. [PubMed: 18492904]
94. Cho SH, Lee JY, Han JK, Choi BI. Acoustic radiation force impulse elastography for the evaluation of focal solid hepatic lesions: preliminary findings. Ultrasound Med Biol. 2010; 36:202–208. [PubMed: 20018432]
95. Doblas, S.; Garteiser, P.; Haddad, N., et al. Magnetic resonance elastography measurements of viscosity: a novel biomarker for human hepatic tumor malignancy?. Proceedings of the 19th Annual Meeting of ISMRM; Montreal, Quebec, Canada. 2011. p. 389
96. Daire, JL.; Sinkus, R.; Wagner, M.; Haddad, N.; Vilgrain, V.; Beers, BV. Is shear viscosity a sign for malignancy in liver tumours?. Proceedings of the 18th Annual Meeting of ISMRM; Stockholm, Sweden. 2010. p. 4658
97. Toubia N, Sanyal AJ. Portal hypertension and variceal hemorrhage. Med Clin North Am. 2008; 92:551–574. [PubMed: 18387376]
98. Vizzutti F, Arena U, Romanelli RG, et al. Liver stiffness measurement predicts severe portal hypertension in patients with HCV-related cirrhosis. Hepatology. 2007; 45:1290–1297. [PubMed: 17464971]
99. Bureau C, Metivier S, Peron JM, et al. Transient elastography accurately predicts presence of significant portal hypertension in patients with chronic liver disease. Aliment Pharmacol Ther. 2008; 27:1261–1268. [PubMed: 18397389]
100. Kazemi F, Kettaneh A, N'Kontchou G, et al. Liver stiffness measurement selects patients with cirrhosis at risk of bearing large oesophageal varices. J Hepatol. 2006; 45:230–235. [PubMed: 16797100]
101. Millonig G, Friedrich S, Adolf S, et al. Liver stiffness is directly influenced by central venous pressure. J Hepatol. 2010; 52:206–210. [PubMed: 20022130]
102. Mannelli L, Godfrey E, Joubert I, et al. MR elastography: spleen stiffness measurements in healthy volunteers--preliminary experience. AJR Am J Roentgenol. 2010; 195:387–392. [PubMed: 20651194]
103. Talwalkar JA, Yin M, Venkatesh S, et al. Feasibility of in vivo MR elastographic splenic stiffness measurements in the assessment of portal hypertension. AJR Am J Roentgenol. 2009; 193:122–127. [PubMed: 19542403]
104. Yin, M.; Talwalkar, JA.; Venkatesh, SK.; Ehman, RL. MR elastography of dynamic postprandial hepatic stiffness augmentation in chronic liver disease. Proceedings of the 17th Annual Meeting of ISMRM; Honolulu, HI. 2009. p. 110

105. Hines, CDG.; Lindstrom, MJ.; Reeder, SB. Effects of posprandial state and mesenteric blood flow on the repeatibility of magnetic resonance elastography. Proceedings of the 18th Annual Meeting of ISMRM; Stockholm, Sweden. 2010. p. 2611

106. Yin, M.; Glaser, KJ.; Kolipaka, A., et al. Influence of perfusion on tissue stiffness assessed with MR elastography. Proceedings of the 18th Annual Meeting of ISMRM; Stockholm, Sweden. 2010. p. 256

107. Jemal A, Siegel R, Ward E, Hao Y, Xu J, Thun MJ. Cancer statistics, 2009. CA Cancer J Clin. 2009; 59:225–249. [PubMed: 19474385]

108. American Cancer Society. Breast cancer facts & figures. Atlanta, GA: American Cancer Sociery, Inc; 2007–2008. p. 34

109. Kuhl C. The current status of breast MR imaging. Part I. Choice of technique, image interpretation, diagnostic accuracy, and transfer to clinical practice. Radiology. 2007; 244:356–378. [PubMed: 17641361]

110. Kuhl CK. Current status of breast MR imaging. Part 2. Clinical applications. Radiology. 2007; 244:672–691. [PubMed: 17709824]

111. Samani A, Zubovits J, Plewes D. Elastic moduli of normal and pathological human breast tissues: an inversion-technique-based investigation of 169 samples. Phys Med Biol. 2007; 52:1565–1576. [PubMed: 17327649]

112. Krouskop TA, Wheeler TM, Kallel F, Garra BS, Hall T. Elastic moduli of breast and prostate tissues under compression. Ultrason Imaging. 1998; 20:260–274. [PubMed: 10197347]

113. Itoh A, Ueno E, Tohno E, et al. Breast disease: clinical application of US elastography for diagnosis. Radiology. 2006; 239:341–350. [PubMed: 16484352]

114. Schaefer FK, Heer I, Schaefer PJ, et al. Breast ultrasound elastography - results of 193 breast lesions in a prospective study with histopathologic correlation. Eur J Radiol. 2011; 77:450–456. [PubMed: 19773141]

115. Zhi H, Ou B, Luo BM, Feng X, Wen YL, Yang HY. Comparison of ultrasound elastography, mammography, and sonography in the diagnosis of solid breast lesions. J Ultrasound Med. 2007; 26:807–815. [PubMed: 17526612]

116. Cho N, Moon WK, Park JS, Cha JH, Jang M, Seong MH. Nonpalpable breast masses: evaluation by US elastography. Korean J Radiol. 2008; 9:111–118. [PubMed: 18385557]

117. Athanasiou A, Tardivon A, Tanter M, et al. Breast lesions: quantitative elastography with supersonic shear imaging - preliminary results. Radiology. 2010; 256:297–303. [PubMed: 20505064]

118. McKnight AL, Kugel JL, Rossman PJ, Manduca A, Hartmann LC, Ehman RL. MR elastography of breast cancer: preliminary results. AJR Am J Roentgenol. 2002; 178:1411–1417. [PubMed: 12034608]

119. Lorenzen J, Sinkus R, Lorenzen M, et al. MR elastography of the breast:preliminary clinical results. Rofo. 2002; 174:830–834. [PubMed: 12101471]

120. Xydeas T, Siegmann K, Sinkus R, Krainick-Strobel U, Miller S, Claussen CD. Magnetic resonance elastography of the breast: correlation of signal intensity data with viscoelastic properties. Invest Radiol. 2005; 40:412–420. [PubMed: 15973132]

121. Siegmann KC, Xydeas T, Sinkus R, Kraemer B, Vogel U, Claussen CD. Diagnostic value of MR elastography in addition to contrast-enhanced MR imaging of the breast-initial clinical results. Eur Radiol. 2010; 20:318–325. [PubMed: 19727753]

122. Rao G, Fisch L, Srinivasan S, et al. Does this patient have Parkinson disease? JAMA. 2003; 289:347–353. [PubMed: 12525236]

123. Foran JR, Steinman S, Barash I, Chambers HG, Lieber RL. Structural and mechanical alterations in spastic skeletal muscle. Dev Med Child Neurol. 2005; 47:713–717. [PubMed: 16174321]

124. Shinohara M, Sabra K, Gennisson JL, Fink M, Tanter M. Real-time visualization of muscle stiffness distribution with ultrasound shear wave imaging during muscle contraction. Muscle Nerve. 2010; 42:438–441. [PubMed: 20665510]

125. Gennisson JL, Catheline S, Chaffai S, Fink M. Transient elastography in anisotropic medium: application to the measurement of slow and fast shear wave speeds in muscles. J Acoust Soc Am. 2003; 114:536–541. [PubMed: 12880065]

126. Gennisson JL, Deffieux T, Mace E, Montaldo G, Fink M, Tanter M. Viscoelastic and anisotropic mechanical properties of in vivo muscle tissue assessed by supersonic shear imaging. Ultrasound Med Biol. 2010; 36:789–801. [PubMed: 20420970]

127. Nordez A, Hug F. Muscle shear elastic modulus measured using supersonic shear imaging is highly related to muscle activity level. J Appl Physiol. 2010; 108:1389–1394. [PubMed: 20167669]

128. Pislaru C, Urban MW, Nenadic I, Greenleaf JF. Shearwave dispersion ultrasound vibrometry applied to in vivo myocardium. Conf Proc IEEE Eng Med Biol Soc. 2009; 2009:2891–2894. [PubMed: 19964051]

129. Sikdar S, Shah JP, Gebreab T, et al. Novel applications of ultrasound technology to visualize and characterize myofascial trigger points and surrounding soft tissue. Arch Phys Med Rehabil. 2009; 90:1829–1838. [PubMed: 19887205]

130. Deffieux T, Montaldo G, Tanter M, Fink M. Shear wave spectroscopy for in vivo quantification of human soft tissues visco-elasticity. IEEE Trans Med Imaging. 2009; 28:313–322. [PubMed: 19244004]

131. Botar-Jid C, Damian L, Dudea SM, Vasilescu D, Rednic S, Badea R. The contribution of ultrasonography and sonoelastography in assessment of myositis. Med Ultrason. 2010; 12:120–126. [PubMed: 21173939]

132. Hoyt K, Kneezel T, Castaneda B, Parker KJ. Quantitative sonoelastography for the in vivo assessment of skeletal muscle viscoelasticity. Phys Med Biol. 2008; 53:4063–4080. [PubMed: 18612176]

133. Gao L, Parker KJ, Lerner RM, Levinson SF. Imaging of the elastic properties of tissue--a review. Ultrasound Med Biol. 1996; 22:959–977. [PubMed: 9004420]

134. Cespedes I, Ophir J, Ponnekanti H, Maklad N. Elastography: elasticity imaging using ultrasound with application to muscle and breast in vivo. Ultrason Imaging. 1993; 15:73–88. [PubMed: 8346612]

135. Dresner MA, Rose GH, Rossman PJ, Muthupillai R, Manduca A, Ehman RL. Magnetic resonance elastography of skeletal muscle. J Magn Reson Imaging. 2001; 13:269–276. [PubMed: 11169834]

136. Uffmann K, Maderwald S, Ajaj W, et al. In vivo elasticity measurements of extremity skeletal muscle with MR elastography. NMR Biomed. 2004; 17:181–190. [PubMed: 15229931]

137. Jenkyn TR, Ehman RL, An KN. Noninvasive muscle tension measurement using the novel technique of magnetic resonance elastography (MRE). J Biomech. 2003; 36:1917–1921. [PubMed: 14614945]

138. Basford JR, Jenkyn TR, An KN, Ehman RL, Heers G, Kaufman KR. Evaluation of healthy and diseased muscle with magnetic resonance elastography. Arch Phys Med Rehabil. 2002; 83:1530–1536. [PubMed: 12422320]

139. McCullough MB, Domire ZJ, Reed AM, et al. Evaluation of muscles affected by myositis using magnetic resonance elastography. Muscle Nerve. 2011; 43:585–590. [PubMed: 21319167]

140. Domire ZJ, McCullough MB, Chen Q, An KN. Wave attenuation as a measure of muscle quality as measured by magnetic resonance elastography: initial results. J Biomech. 2009; 42:537–540. [PubMed: 19171346]

141. Bensamoun SF, Ringleb SI, Chen Q, Ehman RL, An KN, Brennan M. Thigh muscle stiffness assessed with magnetic resonance elastography in hyperthyroid patients before and after medical treatment. J Magn Reson Imaging. 2007; 26:708–713. [PubMed: 17729336]

142. Chen Q, Basford J, An KN. Ability of magnetic resonance elastography to assess taut bands. Clin Biomech (Bristol, Avon). 2008; 23:623–629.

143. Cheng S, Gandevia SC, Green M, Sinkus R, Bilston LE. Viscoelastic properties of the tongue and soft palate using MR elastography. J Biomech. 2011; 44:450–454. [PubMed: 21040923]

144. Nye, E.; Cheng, S.; Gandevia, S.; McKenzie, D.; Sinkus, R.; Bilston, L. Measuring the change in mechanical properties of upper airway soft tissues in obstructive sleep apnea using magnetic resonance elastography. Proceedings of the 19th Annual Meeting of ISMRM; Montreal, Quebec, Canada. 2011. p. 4286

145. Papazoglou S, Rump J, Braun J, Sack I. Shear wave group velocity inversion in MR elastography of human skeletal muscle. Magn Reson Med. 2006; 56:489–497. [PubMed: 16894586]

146. Klatt D, Papazoglou S, Braun J, Sack I. Viscoelasticity-based MR elastography of skeletal muscle. Phys Med Biol. 2010; 55:6445–6459. [PubMed: 20952814]

147. Cheung YY, Doyley M, Miller TB, et al. Magnetic resonance elastography of the plantar fat pads: preliminary study in diabetic patients and asymptomatic volunteers. J Comput Assist Tomogr. 2006; 30:321–326. [PubMed: 16628057]

148. Papazoglou S, Hamhaber U, Braun J, Sack I. Horizontal shear wave scattering from a nonwelded interface observed by magnetic resonance elastography. Phys Med Biol. 2007; 52:675–684. [PubMed: 17228113]

149. Mariappan YK, Glaser KJ, Manduca A, Ehman RL. Cyclic motion encoding for enhanced MR visualization of slip interfaces. J Magn Reson Imaging. 2009; 30:855–863. [PubMed: 19787735]

150. Mariappan YK, Manduca A, Glaser KJ, Chen J, Amrami KK, Ehman RL. Vibration imaging for localization of functional compartments of the extrinsic flexor muscles of the hand. J Magn Reson Imaging. 2010; 31:1395–1401. [PubMed: 20512892]

151. Di Ieva A, Grizzi F, Rognone E, et al. Magnetic resonance elastography: a general overview of its current and future applications in brain imaging. Neurosurg Rev. 2010; 33:137–145. [PubMed: 20195674]

152. Ge Y. Seeing is believing: in vivo evolution of multiple sclerosis pathology with magnetic resonance. Top Magn Reson Imaging. 2006; 17:295–306. [PubMed: 17415002]

153. Anderson VC, Litvack ZN, Kaye JA. Magnetic resonance approaches to brain aging and Alzheimer disease-associated neuropathology. Top Magn Reson Imaging. 2005; 16:439–452. [PubMed: 17088693]

154. Wahlund LO, Almkvist O, Blennow K, et al. Evidence-based evaluation of magnetic resonance imaging as a diagnostic tool in dementia workup. Top Magn Reson Imaging. 2005; 16:427–437. [PubMed: 17088692]

155. Whitwell JL, Jack CR Jr. Comparisons between Alzheimer disease, frontotemporal lobar degeneration, and normal aging with brain mapping. Top Magn Reson Imaging. 2005; 16:409–425. [PubMed: 17088691]

156. Bastos Leite AJ, Scheltens P, Barkhof F. Pathological aging of the brain: an overview. Top Magn Reson Imaging. 2004; 15:369–389. [PubMed: 16041289]

157. Newton HB, Ray-Chaudhury A, Cavaliere R. Brain tumor imaging and cancer management: the neuro-oncologists perspective. Top Magn Reson Imaging. 2006; 17:127–136. [PubMed: 17198229]

158. Thoman WJ, Ammirati M, Caragine LP Jr, McGregor JM, Sarkar A, Chiocca EA. Brain tumor imaging and surgical management: the neurosurgeon's perspective. Top Magn Reson Imaging. 2006; 17:121–126. [PubMed: 17198228]

159. Essig M, Weber MA, von Tengg-Kobligk H, Knopp MV, Yuh WT, Giesel FL. Contrast-enhanced magnetic resonance imaging of central nervous system tumors: agents, mechanisms, and applications. Top Magn Reson Imaging. 2006; 17:89–106. [PubMed: 17198225]

160. Cha S. CNS tumors: monitoring therapeutic response and outcome prediction. Top Magn Reson Imaging. 2006; 17:63–68. [PubMed: 17198223]

161. Vertinsky AT, Barnes PD. Macrocephaly, increased intracranial pressure, and hydrocephalus in the infant and young child. Top Magn Reson Imaging. 2007; 18:31–51. [PubMed: 17607142]

162. Vappou J, Breton E, Choquet P, Goetz C, Willinger R, Constantinesco A. Magnetic resonance elastography compared with rotational rheometry for in vitro brain tissue viscoelasticity measurement. MAGMA. 2007; 20:273–278. [PubMed: 18080819]

163. Vappou J, Breton E, Choquet P, Willinger R, Constantinesco A. Assessment of in vivo and post-mortem mechanical behavior of brain tissue using magnetic resonance elastography. J Biomech. 2008; 41:2954–2959. [PubMed: 18805534]

164. Atay SM, Kroenke CD, Sabet A, Bayly PV. Measurement of the dynamic shear modulus of mouse brain tissue in vivo by magnetic resonance elastography. J Biomech Eng. 2008; 130:021013. [PubMed: 18412500]

165. Pattison AJ, Lollis SS, Perrinez PR, et al. Time-harmonic magnetic resonance elastography of the normal feline brain. J Biomech. 2010; 43:2747–2752. [PubMed: 20655045]
166. Scholz M, Lorenz A, Pesavento A, et al. Current status of intraoperative real-time vibrography in neurosurgery. Ultraschall Med. 2007; 28:493–497. [PubMed: 17918047]
167. Cheng S, Clarke EC, Bilston LE. Rheological properties of the tissues of the central nervous system: a review. Med Eng Phys. 2008; 30:1318–1337. [PubMed: 18614386]
168. Kruse SA, Rose GH, Glaser KJ, et al. Magnetic resonance elastography of the brain. Neuroimage. 2008; 39:231–237. [PubMed: 17913514]
169. Chatelin S, Constantinesco A, Willinger R. Fifty years of brain tissue mechanical testing: from in vitro to in vivo investigations. Biorheology. 2010; 47:255–276. [PubMed: 21403381]
170. Green MA, Bilston LE, Sinkus R. In vivo brain viscoelastic properties measured by magnetic resonance elastography. NMR Biomed. 2008; 21:755–764. [PubMed: 18457350]
171. Zhang, J.; Green, M.; Sinkus, R.; Bilston, L. Magnetic resonance elastography of the cerebellum. Proceedings of the 19th Annual Meeting of ISMRM; Montreal, Quebec, Canada. 2011. p. 1481
172. Sack I, Beierbach B, Wuerfel J, et al. The impact of aging and gender on brain viscoelasticity. Neuroimage. 2009; 46:652–657. [PubMed: 19281851]
173. Wuerfel J, Paul F, Beierbach B, et al. MR-elastography reveals degradation of tissue integrity in multiple sclerosis. Neuroimage. 2010; 49:2520–2525. [PubMed: 19539039]
174. Streitberger, KJ.; Paul, F.; Krefting, D., et al. Decrease in brain stiffness compared to loss of brain volume in multiple sclerosis patients. Proceedings of the 18th Annual Meeting of ISMRM; Stockholm, Sweden. 2010. p. 383
175. Freimann FB, Streitberger KJ, Klatt D, et al. Alteration of brain viscoelasticity after shunt treatment in normal pressure hydrocephalus. Neuroradiology. 201110.1007/s00234-011-0871-1
176. Murphy, MC.; Huston, J.; Jack, CR., Jr, et al. Decreased brain stiffness in Alzheimer's disease determined by magnetic resonance elastography. Proceedings of the 19th Annual Meeting of ISMRM; Montreal, Quebec, Canada. 2011. p. 690
177. Xu L, Lin Y, Han JC, Xi ZN, Shen H, Gao PY. Magnetic resonance elastography of brain tumors: preliminary results. Acta Radiol. 2007; 48:327–330. [PubMed: 17453505]
178. Hirsch, S.; Streitberger, KJ.; Hoffmann, JR., et al. MR elastography of stroke: a feasibility study. Proceedings of the 18th Annual Meeting of ISMRM; Stockholm, Sweden. 2010. p. 513
179. Latta P, Gruwel ML, Debergue P, Matwiy B, Sboto-Frankenstein UN, Tomanek B. Convertible pneumatic actuator for magnetic resonance elastography of the brain. Magn Reson Imaging. 2011; 29:147–152. [PubMed: 20833495]
180. Rossman, PJ.; Rose, GH.; Riederer, SJ.; Ehman, RL. A local gradient feedback system for use in MR elastography. Proceedings of the 6th Annual Meeting of ISMRM; Sydney, Australia. 1998. p. 2009
181. Gallichan D, Robson MD, Bartsch A, Miller KL. TREMR: table-resonance elastography with MR. Magn Reson Med. 2009; 62:815–821. [PubMed: 19585596]
182. Soellinger M, Rutz AK, Kozerke S, Boesiger P. 3D cine displacement-encoded MRI of pulsatile brain motion. Magn Reson Med. 2009; 61:153–162. [PubMed: 19097224]
183. Zhao, S.; Jackson, A.; Parker, GJ. Auto-elastography of the brain. Proceedings of the 17th Annual Meeting of ISMRM; Honolulu, Hawaii. 2009. p. 713
184. Soellinger, M.; Rutz, AK.; Kozerke, S.; Bjeljac, M.; Boesiger, P. Measurement of pulsatile brain motion in a patient with a meningioma. Proceedings of the 14th Annual Meeting of ISMRM; Seattle, Washington. 2006. p. 1596
185. Soellinger M, Ryf S, Boesiger P, Kozerke S. Assessment of human brain motion using CSPAMM. J Magn Reson Imaging. 2007; 25:709–714. [PubMed: 17347993]
186. Miyati T, Mase M, Kasai H, et al. Noninvasive MRI assessment of intracranial compliance in idiopathic normal pressure hydrocephalus. J Magn Reson Imaging. 2007; 26:274–278. [PubMed: 17610284]
187. Gaasch WH, Zile MR. Left ventricular diastolic dysfunction and diastolic heart failure. Annu Rev Med. 2004; 55:373–394. [PubMed: 14746527]

188. Zieman SJ, Melenovsky V, Kass DA. Mechanisms, pathophysiology, and therapy of arterial stiffness. Arterioscler Thromb Vasc Biol. 2005; 25:932–943. [PubMed: 15731494]

189. Burkhoff D, Mirsky I, Suga H. Assessment of systolic and diastolic ventricular properties via pressure-volume analysis: a guide for clinical, translational, and basic researchers. Am J Physiol Heart Circ Physiol. 2005; 289:H501–512. [PubMed: 16014610]

190. Moore CC, McVeigh ER, Zerhouni EA. Quantitative tagged magnetic resonance imaging of the normal human left ventricle. Top Magn Reson Imaging. 2000; 11:359–371. [PubMed: 11153703]

191. Lee WN, Qian Z, Tosti CL, Brown TR, Metaxas DN, Konofagou EE. Preliminary validation of angle-independent myocardial elastography using MR tagging in a clinical setting. Ultrasound Med Biol. 2008; 34:1980–1997. [PubMed: 18952364]

192. Haraldsson H, Wigstrom L, Lundberg M, et al. Improved estimation and visualization of two-dimensional myocardial strain rate using MR velocity mapping. J Magn Reson Imaging. 2008; 28:604–611. [PubMed: 18777541]

193. Konofagou EE, D'Hooge J, Ophir J. Myocardial elastography - a feasibility study in vivo. Ultrasound Med Biol. 2002; 28:475–482. [PubMed: 12049961]

194. Lee WN, Provost J, Fujikura K, Wang J, Konofagou EE. In vivo study of myocardial elastography under graded ischemia conditions. Phys Med Biol. 2011; 56:1155–1172. [PubMed: 21285479]

195. Filusch A, Mereles D, Gruenig E, Buss S, Katus HA, Meyer FJ. Strain and strain rate echocardiography for evaluation of right ventricular dysfunction in patients with idiopathic pulmonary arterial hypertension. Clin Res Cardiol. 2010; 99:491–498. [PubMed: 20352437]

196. Hsu SJ, Bouchard RR, Dumont DM, Wolf PD, Trahey GE. In vivo assessment of myocardial stiffness with acoustic radiation force impulse imaging. Ultrasound Med Biol. 2007; 33:1706–1719. [PubMed: 17698282]

197. Pernot M, Fujikura K, Fung-Kee-Fung SD, Konofagou EE. ECG-gated, mechanical and electromechanical wave imaging of cardiovascular tissues in vivo. Ultrasound Med Biol. 2007; 33:1075–1085. [PubMed: 17507146]

198. Kanai H. Propagation of spontaneously actuated pulsive vibration in human heart wall and in vivo viscoelasticity estimation. IEEE Trans Ultrason Ferroelectr Freq Control. 2005; 52:1931–1942. [PubMed: 16422405]

199. Kanai H. Propagation of vibration caused by electrical excitation in the normal human heart. Ultrasound Med Biol. 2009; 35:936–948. [PubMed: 19251357]

200. Wen H, Bennett E, Epstein N, Plehn J. Magnetic resonance imaging assessment of myocardial elastic modulus and viscosity using displacement imaging and phase-contrast velocity mapping. Magn Reson Med. 2005; 54:538–548. [PubMed: 16086299]

201. Rump J, Klatt D, Braun J, Warmuth C, Sack I. Fractional encoding of harmonic motions in MR elastography. Magn Reson Med. 2007; 57:388–395. [PubMed: 17260354]

202. Sack I, Rump J, Elgeti T, Samani A, Braun J. MR elastography of the human heart: noninvasive assessment of myocardial elasticity changes by shear wave amplitude variations. Magn Reson Med. 2009; 61:668–677. [PubMed: 19097236]

203. Elgeti T, Rump J, Hamhaber U, et al. Cardiac magnetic resonance elastography. initial results. Invest Radiol. 2008; 43:762–772. [PubMed: 18923255]

204. Elgeti T, Laule M, Kaufels N, et al. Cardiac MR elastography: comparison with left ventricular pressure measurement. J Cardiovasc Magn Reson. 2009; 11:44. [PubMed: 19900266]

205. Elgeti T, Beling M, Hamm B, Braun J, Sack I. Cardiac magnetic resonance elastography: toward the diagnosis of abnormal myocardial relaxation. Invest Radiol. 201010.1097/rli.0b013e3181ec4b63

206. Elgeti T, Beling M, Hamm B, Braun J, Sack I. Elasticity-based determination of isovolumetric phases in the human heart. J Cardiovasc Magn Reson. 2010; 12:60. [PubMed: 20979648]

207. Kolipaka, A.; Araoz, PA.; McGee, KP.; Manduca, A.; Ehman, RL. In vivo cardiac MR elastography in a single breath hold. Proceedings of the 18th Annual Meeting of ISMRM; Stockholm, Sweden. 2010. p. 591

208. Kolipaka A, Araoz PA, McGee KP, Manduca A, Ehman RL. Magnetic resonance elastography as a method for the assessment of effective myocardial stiffness throughout the cardiac cycle. Magn Reson Med. 2010; 64:862–870. [PubMed: 20578052]

209. Kolipaka A, McGee KP, Manduca A, Anavekar N, Ehman RL, Araoz PA. In vivo assessment of MR elastography-derived effective end-diastolic myocardial stiffness under different loading conditions. J Magn Reson Imaging. 2011; 33:1224–1228. [PubMed: 21509882]

210. Robert, B.; Sinkus, R.; Gennisson, JL.; Fink, M. Application of DENSE MR-Elastography to the human heart: first in vivo results. Proceedings of the 17th Annual Meeting of ISMRM; Honolulu, HI. 2009. p. 711

211. Robert B, Sinkus R, Gennisson JL, Fink M. Application of DENSE-MR-elastography to the human heart. Magn Reson Med. 2009; 62:1155–1163. [PubMed: 19780150]

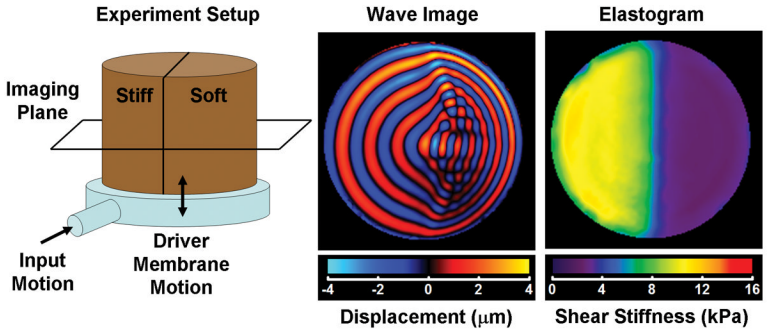

Figure 1.

The diagram on the left depicts an MRE experiment performed on a 2-layer bovine gelatin phantom made of a stiff gel and a soft gel. The phantom rests on a plastic drum driver supplied with time-harmonic pressure variations that flex the membrane of the driver. As the phantom shakes up and down, shear waves are produced at the edge of the phantom (due to inertial effects) that propagate into the phantom. The phantom was imaged in the coronal imaging plane. The middle image shows a wave image from an MRE acquisition performed with motion encoding in the through-plane direction. The difference in the shear wavelength in the two regions is evident with the wavelength being longer in the stiff region. The image on the right is an elastogram of the phantom indicating the stiff and soft regions.

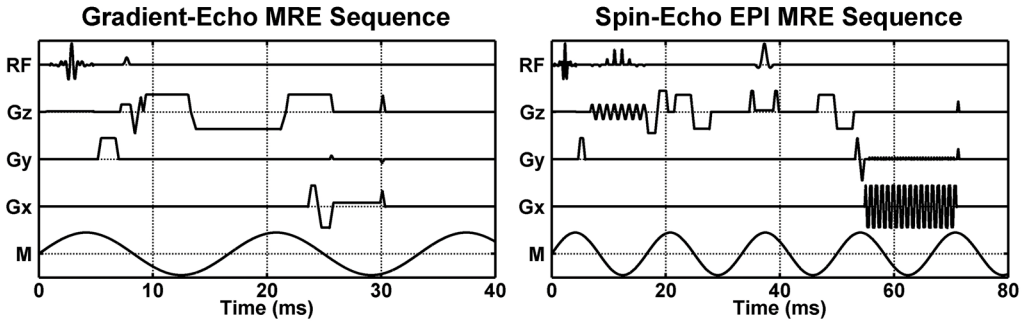

Figure 2.

MRE pulse sequence diagrams are shown depicting the RF pulses; gradients in the frequency-encoding, phase-encoding, and slice-select directions; and the applied motion (RF, Gx, Gy, Gz, and M, respectively). On the left is a GRE MRE sequence for imaging 60-Hz mechanical motion using a 16.7-ms gradient-moment-nulled (GMN) motion-encoding gradient (MEG) applied along Gz. On the right is a SE-EPI MRE sequence for imaging 60-Hz motion using 2 bipolar 6.5-ms MEG, 1 on each side of the refocusing pulse and synchronized to the motion. Both sequences are shown with GMN imaging gradients and spatial presaturation pulses.

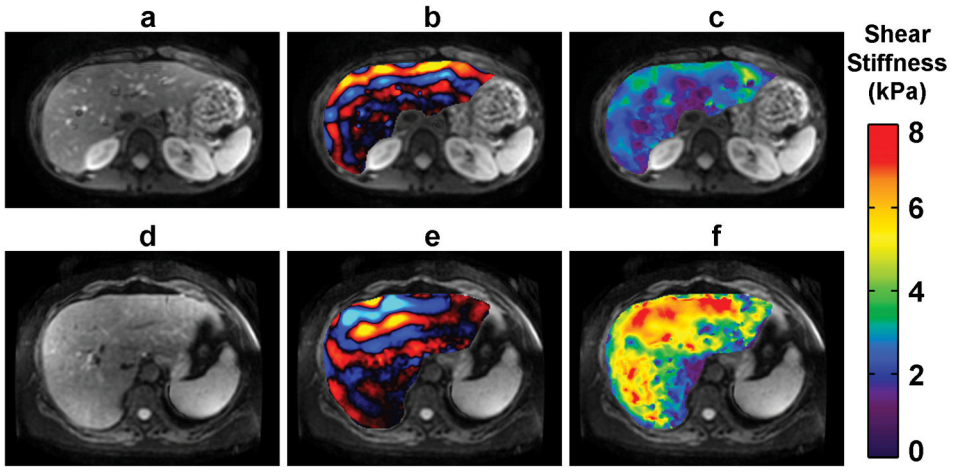

Figure 3.

Hepatic MRE exams of a 28-year-old healthy female volunteer with no known liver disease (top row) and a 66-year-old female with steatohepatitis with bridging fibrosis, early cirrhosis grade 3–4, and stage-2 inflammation (bottom row). Anatomical reference images are shown in (a) and (d), MRE wave images are shown in (b) and (e), and the MRE elastograms are shown in (c) and (f). The fibrotic liver can be seen to be significantly stiffer than the healthy liver. (Courtesy of Dr. Meng Yin, Mayo Clinic, Rochester, MN.)

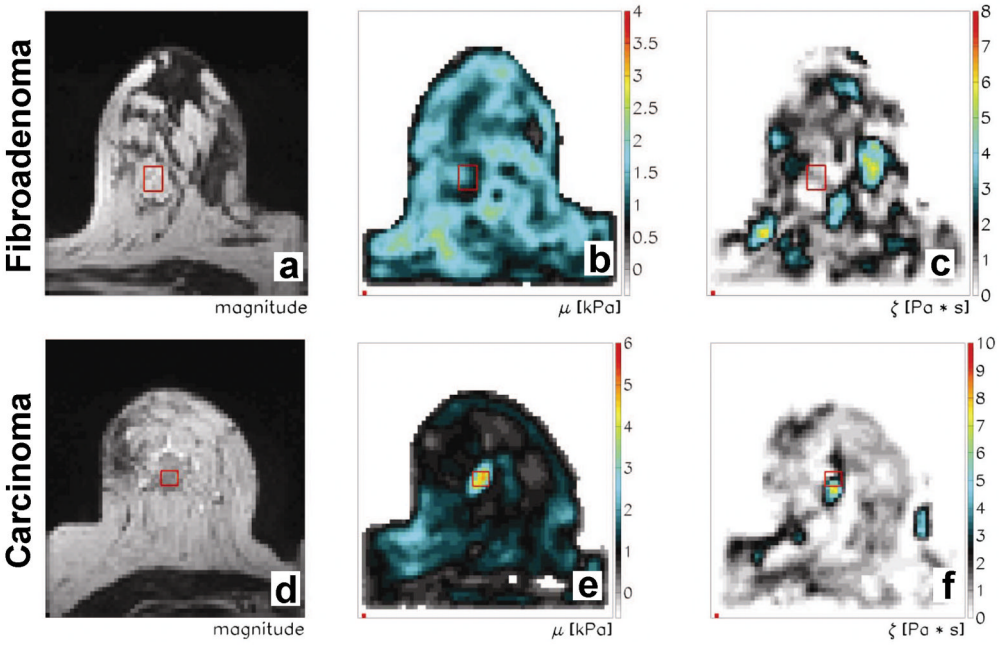

Figure 4.

Breast MRE images from exams performed on patients with a fibroadenoma (top row) and an invasive carcinoma (bottom row). The acquisitions were performed using 65-Hz vibrations applied to the lateral side of the breast. MR magnitude images from the MRE acquisition are shown in the first column, while shear stiffness and viscosity images from the MRE reconstruction are shown in the second and third columns, respectively. (From Xydeas T, Siegmann K, Sinkus R, Krainick-Strobel U, Miller S, Claussen CD. Magnetic resonance elastography of the breast: correlation of signal intensity data with viscoelastic properties. Invest Radiol 2005;40(7):412–420, adapted with permission.)

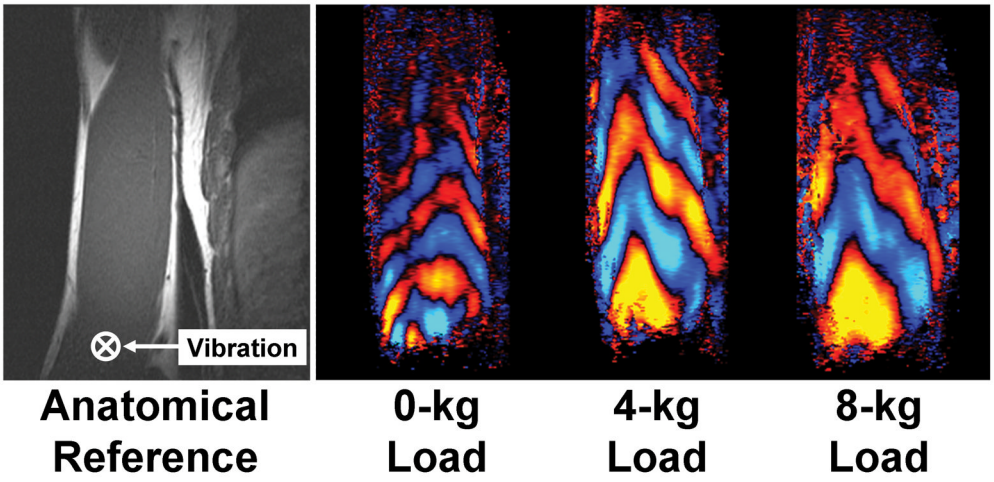

Figure 5.

MRE investigation of stiffness changes in the loaded and unloaded biceps brachii. The MRE acquisition of the right arm was performed on a healthy male subject lying in the right lateral decubitus position as described in Dresner et al. (135). The subject was imaged in a coronal plane while supporting different amounts of weight. The image on the left is a reference image indicating the orientation of the muscle and the location of the driver, which was placed above the distal biceps tendon and vibrated in the through-plane direction. The three images on the right show wave images from the MRE acquisitions performed with the subject holding 0-, 4-, and 8-kg loads. The shear wavelength in the muscle can be seen to increase with the increasing muscle load, indicating that the stiffness of the muscle has significantly increased. (Courtesy of Dr. Yogesh Mariappan, Mayo Clinic, Rochester, MN.)

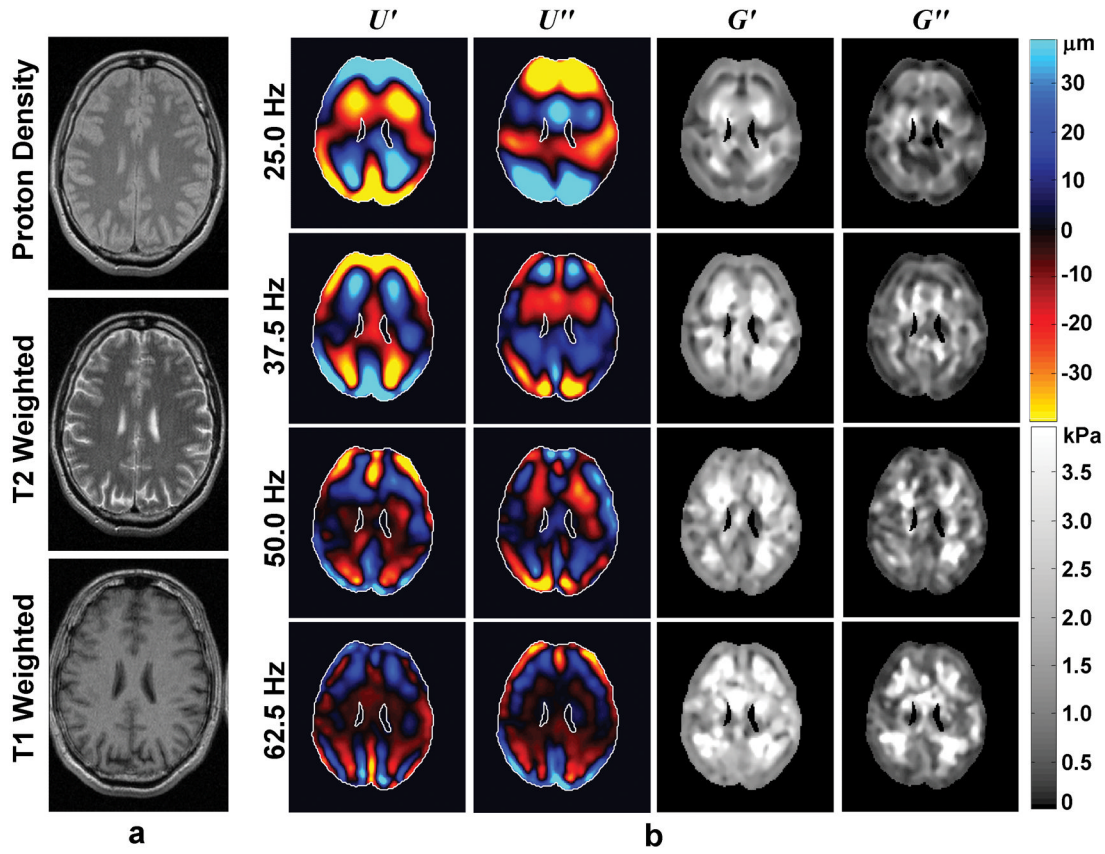

Figure 6.

Example of brain MRE performed on a 47-year-old healthy male volunteer. (a) Proton-density-weighted, T2-weighted, and T1-weighted anatomical MR images. (b) Wave images and elastograms for data corresponding to several frequencies of mechanical vibration ranging from 25 Hz (top row) to 62.5 Hz (bottom row). The first two columns show the real and imaginary parts of the wave data obtained at each frequency, and the last two columns show the real and imaginary parts of the reconstructed shear moduli at each frequency. (From Sack I, Beierbach B, Wuerfel J, et al. The impact of aging and gender on brain viscoelasticity. Neuroimage 2009;46(3):652–657, adapted with permission.)

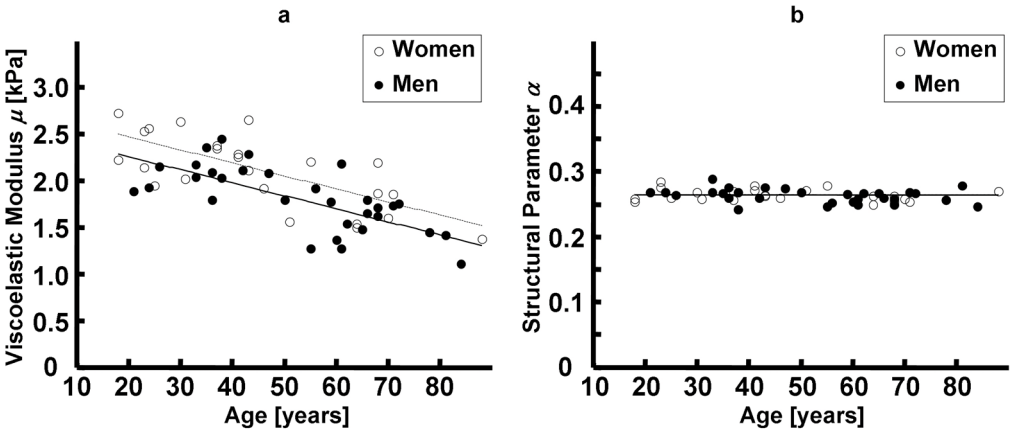

Figure 7.

Changes in brain tissue mechanical properties with age and gender in an MRE study of 55 healthy subjects (23 females, 32 males). (a) The viscoelastic modulus obtained from a spring-pot model of multifrequency MRE data shows a decline in brain tissue stiffness at about 0.8% per year with female brain stiffness being slightly higher than the age-matched male subjects. (b) The structural parameter derived from the spring-pot model does not appear to vary with age or sex. (From Sack I, Beierbach B, Wuerfel J, et al. The impact of aging and gender on brain viscoelasticity. Neuroimage 2009;46(3):652–657, adapted with permission.)

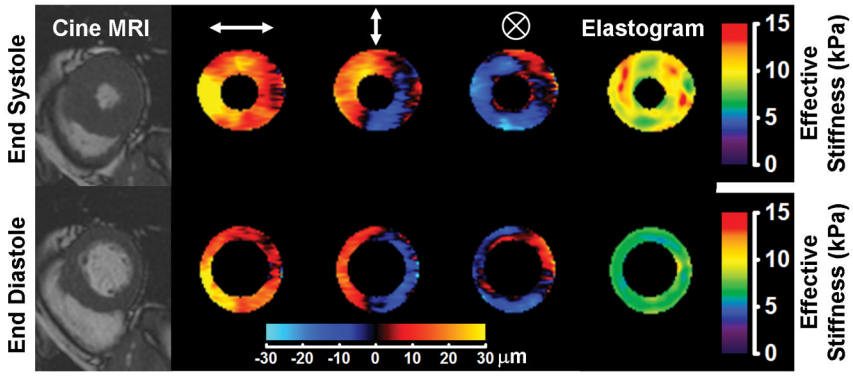

Figure 8.

Cardiac MRE performed in a healthy volunteer as described in Kolipaka et al. (207). The subject was imaged in the supine position with 80-Hz vibrations induced in the heart via a pneumatic driver system placed against the chest wall anterior to the heart. Measurements were performed of the short axis of the left ventricle at the end of systole and the end of diastole. The left column shows MR images from a cine acquisition showing the anatomy of the left ventricle at these phases of the cardiac cycle. Columns 2, 3, and 4 show masked wave images of the horizontal, vertical, and though-plane components of the motion, respectively, produced in the heart. Column 5 shows the elastograms produced from the wave data. The cardiac tissue can be seen to be significantly stiffer at the end of systole than at the end of diastole. (Courtesy of Dr. Arunark Kolipaka, The Ohio State University Medical Center, Columbus, OH.)

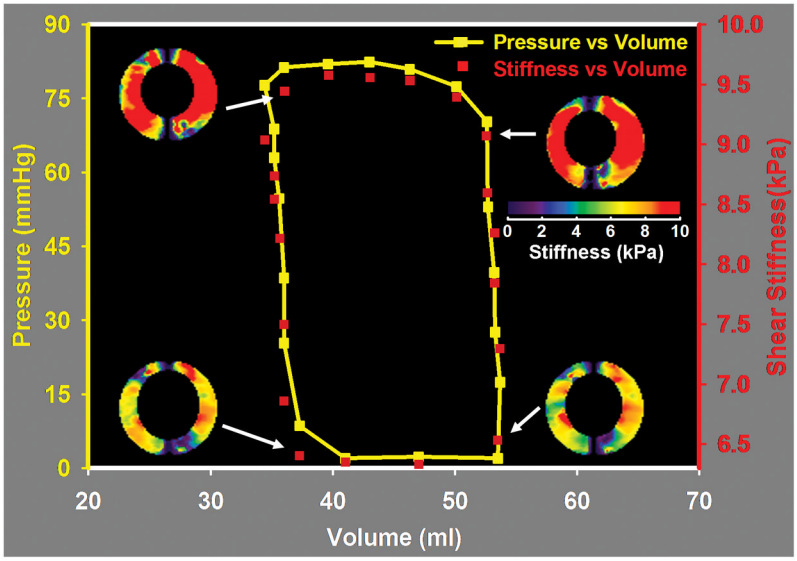

Figure 9.

Cardiac MRE performed in vivo in a normal pig as described in Kolipaka et al. (208). The pig was imaged in the supine position with a pneumatic drum driver operating at 80 Hz placed above the heart. Data were acquired in a short axis view of the left ventricle while simultaneous measurements of the left ventricular pressure were made. Volume measurements of the left ventricle were performed using separate multislice cine bSSFP acquisitions of the heart. The figure shows the stiffness, pressure, and volume measurements indicating that the measured stiffness correlates well with the changes in ventricular pressure during the cardiac cycle and suggesting that noninvasive stiffness-volume curves obtained with MRE may provide similar information about cardiac function as invasive pressure-volume measurements. (Courtesy of Dr. Arunark Kolipaka, The Ohio State University Medical Center, Columbus, OH.)